PHYSICAL REVIEW D **90,** 074501 (2014)

Baryon spectrum with $N_f = 2 + 1 + 1$ twisted mass fermions

C. Alexandrou,[1,2] V. Drach,[3,4] K. Jansen,[3] C. Kallidonis,[2] and G. Koutsou[2]

[1]*Department of Physics, University of Cyprus, P.O. Box 20537, 1678 Nicosia, Cyprus*
[2]*Computation-based Science and Technology Research Center, The Cyprus Institute, 20 Kavafi Street, Nicosia 2121, Cyprus*
[3]*NIC, DESY, Platanenallee 6, D-15738 Zeuthen, Germany*
[4]*CP^3-Origins and the Danish Institute for Advanced Study DIAS, University of Southern Denmark, Campusvej 55, DK-5230 Odense M, Denmark*

(Received 10 July 2014; published 2 October 2014)

The masses of the low-lying baryons are evaluated using a total of ten ensembles of dynamical twisted mass fermion gauge configurations. The simulations are performed using two degenerate flavors of light quarks, and a strange and a charm quark fixed to approximately their physical values. The light sea quarks correspond to pseudo scalar masses in the range of about 210 to 430 MeV. We use the Iwasaki improved gluonic action at three values of the coupling constant corresponding to lattice spacing $a = 0.094$, 0.082 and 0.065 fm determined from the nucleon mass. We check for both finite volume and cutoff effects on the baryon masses. We examine the issue of isospin symmetry breaking for the octet and decuplet baryons and its dependence on the lattice spacing. We show that in the continuum limit isospin breaking is consistent with zero, as expected. We performed a chiral extrapolation of the forty baryon masses using SU(2) χPT. After taking the continuum limit and extrapolating to the physical pion mass our results are in good agreement with experiment. We provide predictions for the mass of the doubly charmed Ξ_{cc}^*, as well as of the doubly and triply charmed Ωs that have not yet been determined experimentally.

DOI: 10.1103/PhysRevD.90.074501 PACS numbers: 11.15.Ha, 12.38.Gc, 12.38.Aw, 12.38.-t

I. INTRODUCTION

Simulations of QCD defined on four-dimensional Euclidean lattice using near to physical values of the light quark masses are enabling the reliable extraction of the masses of the low-lying hadrons. This progress in lattice QCD coupled with the interest in charmed-baryon spectroscopy, partly triggered by the first observation of a family of doubly charmed baryons $\Xi_{cc}^+(3519)$ and $\Xi_{cc}^{++}(3460)$ by the SELEX Collaboration [1–3], make the study of the charmed hadron masses particularly timely. The fact that the observation of $\Xi_{cc}^+(3519)$ or $\Xi_{cc}^{++}(3460)$, has not be confirmed by the *BABAR* [4] nor the BELLE [5] experiments calls for further attention into the existence of doubly charmed Ξs. Even more interesting is the mass splitting of about 60 MeV for this doublet as compared to the splitting of other previously observed isospin partners that have mass differences 1 order of magnitude smaller. Theoretical studies using e.g. the nonrelativistic [6] and relativistic quark models [7,8], and QCD sum rules [9] predict the Ξ_{cc} mass to be 100–200 MeV higher than that observed by SELEX. Heavy baryon spectra will be further studied experimentally at the recently upgraded Beijing Electron-Positron Collider detector, the Beijing Spectrometer and at the antiproton annihilation at DArmstadt at FAIR. Lattice QCD calculations can provide theoretical input for these experiments. A number of lattice QCD studies have recently looked at the mass of charmed baryons. Most of these studies employ a mixed action approach using staggered sea quarks. In Ref. [10] $N_f = 2 + 1 + 1$ staggered sea quarks with clover light and strange valence quarks and a relativistic action for the charm quark are employed and the results are extrapolated to the continuum limit. In Refs. [11,12] $N_f = 2 + 1$ staggered sea quarks are used with staggered light and strange [11] or domain wall [12] valence quarks with a relativistic action for the charm quark.

In this work we extend our previous study on the low-lying spectrum of the baryon octet and decuplet using $N_f = 2$ twisted mass fermions [13] to $N_f = 2 + 1 + 1$ twisted mass fermions at maximal twist. For the valence strange and charm sector we use an Osterwalder-Seiler quarks avoiding mixing between these two sectors. The strange and charm valence quark masses are tuned using the Ω^- and Λ_c baryon mass, respectively. We analyze a total of ten $N_f = 2 + 1 + 1$ ensembles at three different lattice spacings and volumes. This enables us to take the continuum limit and assess volume effects. Our results are fully compatible with an $\mathcal{O}(a^2)$ behavior which is used to extrapolate to the continuum limit.

The good precision of our results on the baryon masses allows us to perform a study of chiral extrapolations to obtain results at the physical point. This study shows that one of the main uncertainties in predicting the mass at the physical point is caused by the chiral extrapolations, which yield the largest systematic error.

An important issue is the restoration of the explicitly broken isospin symmetry in the continuum limit. At finite lattice spacing, baryon masses display $\mathcal{O}(a^2)$ isospin

breaking effects. There are, however, theoretical arguments [14] as well as numerical evidence [15,16] that these isospin breaking effects are particularly pronounced for the neutral pseudo scalar mass, whereas for other quantities studied so far by the European Twisted Mass Collaboration (ETMC) they are compatible with zero. In this paper, we will corroborate this result also in the baryon sector showing that isospin breaking effects are in general small or even compatible with zero. For a preliminary account of these results see Ref. [17].

The paper is organized as follows: The details of our lattice setup, namely those concerning the twisted mass action, the parameters of the simulations and the interpolating fields used, are given in Sec. II. Section III contains the numerical results of the baryon masses computed for different lattice volumes, lattice spacings and bare quark masses. Lattice artifacts, including finite volume and discretization errors are also discussed with special emphasis on the $\mathcal{O}(a^2)$ isospin breaking effects inherent in the twisted mass formulation of lattice QCD. The chiral extrapolations are analyzed in Sec. IV. Section V contains a comparison with other existing calculations and conclusions are finally drawn in Sec. VI.

II. LATTICE TECHNIQUES

A. The lattice action

In the present work we employ the twisted mass fermion action [18] and the Iwasaki improved gauge action [19]. Twisted mass fermions provide an attractive formulation of lattice QCD that allows for automatic $\mathcal{O}(a)$ improvement, infrared regularization of small eigenvalues and fast dynamical simulations [20].

The twisted mass Wilson action used for the light degenerate doublet of quarks (u, d) is given by [18,20]

$$S_F^{(l)}[\chi^{(l)},\bar{\chi}^{(l)},U] = a^4\sum_x \bar{\chi}^{(l)}(x)(D_W[U] + m_{0,l} + i\mu_l\gamma_5\tau^3)\chi^{(l)}(x) \quad (1)$$

with τ^3 the third Pauli matrix acting in the flavor space, $m_{0,l}$ the bare untwisted light quark mass, μ_l the bare twisted light quark mass and the massless Wilson-Dirac operator given by

$$D_W[U] = \frac{1}{2}\gamma_\mu(\nabla_\mu + \nabla^*_\mu) - \frac{ar}{2}\nabla_\mu\nabla^*_\mu \quad (2)$$

where

$$\nabla_\mu\psi(x) = \frac{1}{a}[U^\dagger_\mu(x)\psi(x+a\hat{\mu}) - \psi(x)] \quad \text{and}$$
$$\nabla^*_\mu\psi(x) = -\frac{1}{a}[U_\mu(x-a\hat{\mu})\psi(x-a\hat{\mu}) - \psi(x)]. \quad (3)$$

The quark fields denoted by $\chi^{(l)}$ in Eq. (1) are in the so-called "twisted basis." The fields in the "physical basis," $\psi^{(l)}$, are obtained for maximal twist by the simple transformation

$$\psi^{(l)}(x) = \frac{1}{\sqrt{2}}(\mathbb{1} + i\tau^3\gamma_5)\chi^{(l)}(x),$$
$$\bar{\psi}^{(l)}(x) = \bar{\chi}^{(l)}(x)\frac{1}{\sqrt{2}}(\mathbb{1} + i\tau^3\gamma_5). \quad (4)$$

In addition to the light sector, a twisted heavy mass-split doublet $\chi^{(h)} = (\chi_c, \chi_s)$ for the strange and charm quarks is introduced, described by the action [21,22]

$$S_F^{(h)}[\chi^{(h)},\bar{\chi}^{(h)},U] = a^4\sum_x \bar{\chi}^{(h)}(x)(D_W[U] + m_{0,h} + i\mu_\sigma\gamma_5\tau^1 + \tau^3\mu_\delta)\chi^{(h)}(x) \quad (5)$$

where $m_{0,h}$ is the bare untwisted quark mass for the heavy doublet, μ_σ is the bare twisted mass along the τ^1 direction and μ_δ is the mass splitting in the τ^3 direction. The quark fields for the heavy quarks in the physical basis are obtained from the twisted basis through the transformation

$$\psi^{(h)}(x) = \frac{1}{\sqrt{2}}(\mathbb{1} + i\tau^1\gamma_5)\chi^{(h)}(x),$$
$$\bar{\psi}^{(h)}(x) = \bar{\chi}^{(h)}(x)\frac{1}{\sqrt{2}}(\mathbb{1} + i\tau^1\gamma_5). \quad (6)$$

In this paper, unless otherwise stated, the quark fields will be understood as "physical fields," ψ, in particular when we define the baryonic interpolating fields.

The form of the fermionic action in Eq. (1) breaks parity and isospin at nonvanishing lattice spacing. In particular, the isospin breaking in physical observables is a cutoff effect of $\mathcal{O}(a^2)$ [20].

Maximally twisted Wilson quarks are obtained by setting the untwisted quark mass m_0 to its critical value $m_{\rm cr}$, while the twisted quark mass parameter μ is kept nonvanishing in order to work away from the chiral limit. A crucial advantage of the twisted mass formulation is the fact that, by tuning the bare untwisted quark mass m_0 to its critical value $m_{\rm cr}$, all physical observables are automatically $\mathcal{O}(a)$ improved [20,22]. In practice, we implement maximal twist of Wilson quarks by tuning to zero the bare untwisted current quark mass, commonly called Partially Conserved Axial Current (PCAC) mass, $m_{\rm PCAC}$ [23,24], which is proportional to $m_0 - m_{\rm cr}$ up to $\mathcal{O}(a)$ corrections. A convenient way to evaluate $m_{\rm PCAC}$ is through

$$m_{\rm PCAC} = \lim_{t/a\gg 1}\frac{\sum_{\mathbf{x}}\langle\partial_4\tilde{A}^b_4(\mathbf{x},t)\tilde{P}^b(0)\rangle}{\sum_{\mathbf{x}}\langle\tilde{P}^b(\mathbf{x},t)\tilde{P}^b(0)\rangle} \quad b = 1,2, \quad (7)$$

where $\tilde{A}^b_\mu = \bar{\chi}\gamma_\mu\gamma_5\frac{\tau^b}{2}\chi$ is the axial vector current and $\tilde{P}^b = \bar{\chi}\gamma_5\frac{\tau^b}{2}\chi$ is the pseudoscalar density in the twisted basis. The large t/a limit is required in order to isolate the contribution of the lowest-lying charged pseudoscalar meson state in the

TABLE I. Input parameters $(\beta, L, a\mu)$ of our lattice simulations with the corresponding lattice spacing (a), pion mass (m_π) as well as the number of gauge configurations analyzed.

	$\beta = 1.90$, $a = 0.0936(13)$ fm $r_0/a = 5.231(38)$				
$32^3 \times 64$, $L = 3.0$ fm	$a\mu$	0.0030	0.0040	0.0050	
	Number of configurations	200	200	200	
	m_π (GeV)	0.261	0.298	0.332	
	$m_\pi L$	3.97	4.53	5.05	
	$\beta = 1.95$, $a = 0.0823(10)$ fm, $r_0/a = 5.710(41)$				
$32^3 \times 64$, $L = 2.6$ fm	$a\mu$	0.0025	0.0035	0.0055	0.0075
	Number of configurations	200	200	200	200
	m_π (GeV)	0.256	0.302	0.372	0.432
	$m_\pi L$	3.42	4.03	4.97	5.77
	$\beta = 2.10$, $a = 0.0646(7)$ fm $r_0/a = 7.538(58)$				
$48^3 \times 96$, $L = 3.1$ fm	$a\mu$	0.0015	0.002	0.003	
	Number of configurations	196	184	200	
	m_π (GeV)	0.213	0.246	0.298	
	$m_\pi L$	3.35	3.86	4.69	

correlators of Eq. (7). This way of determining $m_{\rm PCAC}$ is equivalent to imposing on the lattice the validity of the axial Ward identity $\partial_\mu \tilde{A}^b_\mu = 2m_{\rm PCAC}\tilde{P}^b$, $b = 1, 2$, between the vacuum and the charged zero three-momentum one-pion state. When m_0 is taken such that $m_{\rm PCAC}$ vanishes, this Ward identity expresses isospin conservation, as it becomes clear by rewriting it in the physical quark basis. The value of $m_{\rm cr}$ is determined at each μ_l in our $N_f = 2 + 1 + 1$ simulations, a procedure that preserves $\mathcal{O}(a)$ improvement and keeps $\mathcal{O}(a^2)$ small [23,24]. The reader can find more details on the twisted mass fermion action in Ref. [25]. Simulating a charm quark may give rise to concerns regarding cutoff effects. An analysis presented in Ref. [26] shows that they are surprising small. In this work we investigate in detail the cutoff effects on the hyperon and charmed-baryon masses using simulations at our three values of the lattice spacings. All final results are extrapolated to the continuum limit.

In order to avoid complications due to flavor mixing in the heavy quark sector we only use Osterwalder-Seiler valence strange and charm quarks. Since the bare heavy quark masses in the sea were approximately tuned to the mass of the kaon and D-meson, in order to match their masses exactly tuning would have been required even if we used twisted mass quarks for the strange and the charm. Since our interest in this work is the baryon spectrum we choose to use the physical mass of the Ω^- and the Λ_c in order to tune the Osterwalder-Seiler strange and charm quark masses. This means that we need to choose a value of strange (charm) quark mass performed the computation at several values of the pion mass and then chiral extrapolate the Ω^- (Λ_c) mass and compare with its experimental value. If our chirally extrapolated results do not reproduce the right mass we change the strange (charm) quark mass and iterate until we reach agreement with the experimental value. Osterwalder-Seiler fermions are doublets with $r = \pm 1$ like the u- and d-doublet, i.e. $\chi^{(s)} = (s^+, s^-)$ and $\chi^{(c)} = (c^+, c^-)$, have an action that is the same as for the doublet of light quarks, as given in Eq. (1), but with μ_l in Eq. (1) replaced with the tuned value of the bare twisted mass of the strange (charm) valence quark. Taking m_0 to be equal to the critical mass determined in the light sector the $\mathcal{O}(a)$ improvement in any observable still applies. One can equally work with the upper or the lower component of the strange and charm doublets. In the continuum limit both choices are equivalent. In this work we choose to work with the upper components, namely the s^+ and c^+. The action for the heavy quarks would then read

$$S^{(h)}_{\rm OS}[\chi^{(h)}, \bar{\chi}^{(h)}, U] = a^4 \sum_x \sum_{h=s}^{c} \bar{\chi}^{(h)}(x)(D_W[U] + m_{\rm cr} + i\mu_h\gamma_5)\chi^{(h)}(x). \quad (8)$$

The reader interested in the advantage of this mixed action in the mesonic sector is referred to the Refs. [21,27–30]. We give more details on the tuning of the strange and charm quark masses in Sec. II F.

B. Simulation details

We summarize the input parameters of the calculations, namely β, L/a, the light quark mass $a\mu$ as well as the value of the pion mass in Table I. A total of ten gauge ensembles at three values of β are considered, namely $\beta = 1.90$, $\beta = 1.95$ and $\beta = 2.10$, allowing for an investigation of finite lattice spacing effects and for taking the continuum limit. The values of the lattice spacings a given in Table I are determined using the nucleon mass as explained in Sec. II E. The pion masses for the simulations span a range from about 210 to 430 MeV, which is close enough to the physical point mass to allow us to perform chiral extrapolations.

C. Two-point correlation functions and effective mass

In order to extract baryon masses we consider two-point correlation functions at $\vec{p} = \vec{0}$ defined by

$$C_X^{\pm}(t, \vec{p} = \vec{0}) = \sum_{\mathbf{x}_{\rm sink} - \mathbf{x}_{\rm source}} \left\langle \frac{1}{4} \mathrm{Tr}(1 \pm \gamma_0) \mathcal{J}_X(\mathbf{x}_{\rm sink}, t_{\rm sink}) \times \bar{\mathcal{J}}_X(\mathbf{x}_{\rm source}, t_{\rm source}) \right\rangle, \qquad t = t_{\rm sink} - t_{\rm source} \tag{9}$$

where $\mathcal{J}_X$ is the interpolating field of the baryon state of interest acting at the source $(\mathbf{x}_{\rm source}, t_{\rm source})$ and the sink, $(\mathbf{x}_{\rm sink}, t_{\rm sink})$. Space-time reflection symmetries of the action and the antiperiodic boundary conditions in the temporal direction for the quark fields imply, for zero three-momentum correlators, that $C_X^{+}(t) = -C_X^{-}(T - t)$. Therefore, in order to decrease errors we average correlators in the forward and backward direction and define

$$C_X(t) = C_X^{+}(t) - C_X^{-}(T - t). \tag{10}$$

In addition, the source location is chosen randomly on the whole lattice for each configuration, in order to decrease correlation among measurements.

The ground state mass of a given hadron can be extracted by examining the effective mass defined by

$$\begin{aligned} am_{\rm eff}^X(t) &= \log\left(\frac{C_X(t)}{C_X(t+1)}\right) \\ &= am_X + \log\left(\frac{1 + \sum_{i=1}^{\infty} c_i e^{-\Delta_i t}}{1 + \sum_{i=1}^{\infty} c_i e^{-\Delta_i (t+1)}}\right) \underset{t\to\infty}{\to} am_X \end{aligned} \tag{11}$$

where $\Delta_i = m_i - m_X$ is the mass difference of the excited state i with respect to the ground mass m_X. All results in this work have been extracted from correlators where Gaussian smearing is applied both at the source and sink. In general, effective masses of correlators of any interpolating fields are expected to have the same value in the large time limit, but applying smearing on the interpolating fields suppresses excited states, therefore yielding a plateau region at earlier source-sink time separations and better accuracy in the extraction of the mass. Our fitting procedure to extract m_X is as follows: The sum over excited states in the effective mass given in Eq. (11) is truncated, keeping only the first excited state,

$$am_{\rm eff}^X(t) \approx am_X + \log\left(\frac{1 + c_1 e^{-\Delta_1 t}}{1 + c_1 e^{-\Delta_1 (t+1)}}\right). \tag{12}$$

The upper fitting time slice boundary is kept fixed, while allowing the lower fitting time to be two or three time slices away from $t_{\rm source}$. We then fit the effective mass to the form given in Eq. (12). This exponential fit yields an estimate for c_1 and Δ_1 as well as for the ground state mass, which we denote by $m_X^{(E)}$. Then, we perform a constant fit to the effective mass increasing the initial fitting time t_1. We denote the value extracted by $m_X^{(C)}(t_1)$. The final value of the mass is selected such that the ratio

$$\frac{|am_X^{(C)}(t_1) - am_X^{(E)}|}{am_X^{\rm mean}}, \qquad am_X^{\rm mean} = \frac{am_X^{(C)}(t_1) + am_X^{(E)}}{2} \tag{13}$$

becomes less than 50% the statistical error on $m_X^{(C)}(t_1)$. This criterion is, in most cases, in agreement with $\chi^2/\mathrm{d.o.f.}$ becoming less than unity. In the cases in which this criterion is not satisfied a careful examination of the effective mass is made to ensure that the fit range is in the plateau region. We show representative results of these fits to the effective mass of the baryons Ξ^0 and Ω_c^0 in Fig. 1. The error bands on the constant and exponential fits are obtained using jackknife analysis. As can be seen, the exponential and constant fits yield consistent results in the large time limit.

D. Interpolating fields

The baryon states are created from the vacuum with the use of interpolating fields that are constructed such that they have the quantum numbers of the baryon of interest and reduce to the quark model wave functions in the nonrelativistic limit. We have a four-dimensional flavor space and therefore we consider SU(3) subgroups to visualize baryons under SU(4) symmetry. The baryon states split into a $20'$-plet of spin-$1/2$ states and a 20-plet of spin-$3/2$ states. There also exists a $\bar{4}$-plet, which is not considered in this work. Light, strange and charmed baryons can be classified according to their transformation properties under flavor SU(3) and their charm content. This is shown schematically in Fig. 2 and Fig. 3. The spin-$1/2$ $20'$-plet decomposes into three horizontal levels. The first level is the standard octet of the SU(3) symmetry that has no charm quarks, the $c = 1$ is the second level that splits into two SU(3) multiplets, a **6** containing the Σ_c and a $\bar{\mathbf{3}}$ containing the Λ_c and the Ξ_c and the $c = 2$ **3** multiplet of SU(3) that forms the top level. In a similar way, the 20-plet of spin-$3/2$ baryons contains the standard $c = 0$ decuplet at the lowest level, the $c = 1$ level **6** multiplet of SU(3), the $c = 2$ **3** multiplet and a $c = 3$ singlet at the top of the pyramid. The interpolating fields for these baryons, displayed Fig. 2 and Fig. 3, are collected in the Tables XII and XIII of Appendix A [31–33].

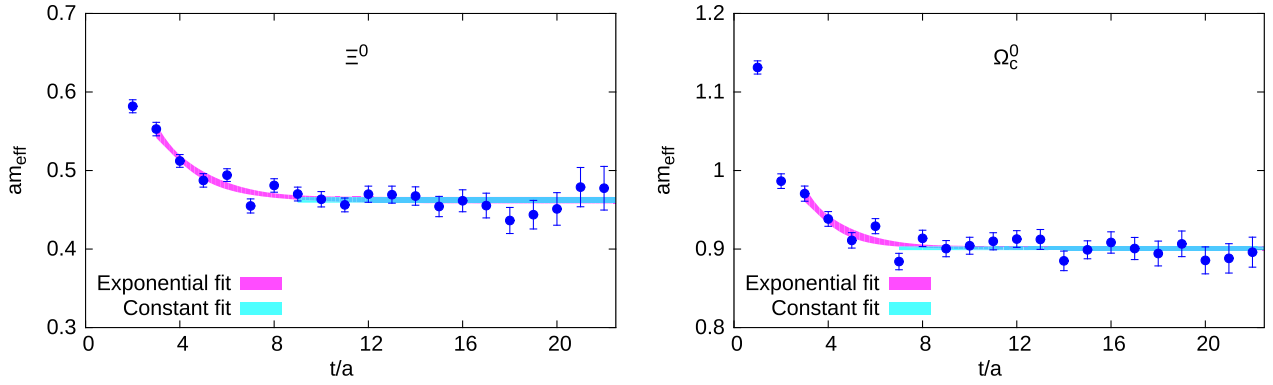

FIG. 1 (color online). Representative effective mass plots for Ξ^0 (left) and Ω_c^0 (right) at $\beta = 2.10$, $a\mu_l = 0.0015$. Both the constant and the exponential fits are displayed.

In other recent works where baryon properties are studied, e.g. in Ref. [34], different interpolating fields to those we provide in Tables XII and XIII were used. These different interpolating fields are tabulated in Table XIV of Appendix A. In what follows we will compare the effective masses using the two different sets that have the same quantum numbers but different structure.

As local interpolating fields are not optimal for suppressing excited state contributions, we apply Gaussian smearing to each quark field $q(\mathbf{x}, t)$ [35,36]. The smeared quark field is given by $q^{\text{smear}}(\mathbf{x}, t) = \sum_y F(\mathbf{x}, \mathbf{y}; U(t)) q(\mathbf{y}, t)$, where we have used the gauge invariant smearing function

$$F(\mathbf{x}, \mathbf{y}; U(t)) = (1 + \alpha H)^n(\mathbf{x}, \mathbf{y}; U(t)), \tag{14}$$

constructed from the hopping matrix understood as a matrix in coordinate, color and spin space,

$$H(\mathbf{x}, \mathbf{y}; U(t)) = \sum_{i=1}^{3} (U_i(\mathbf{x}, t)\delta_{\mathbf{x},\mathbf{y}-a\hat{i}} + U_i^\dagger(\mathbf{x} - a\hat{i}, t)\delta_{\mathbf{x},\mathbf{y}+a\hat{i}}). \tag{15}$$

In addition, we apply APE smearing to the spatial links that enter the hopping matrix. The parameters α and n of the Gaussian and APE smearing at each value of β are collected in Table II.

The interpolating fields for the spin-3/2 baryons defined in Table XIII have an overlap with spin-1/2 states. These overlaps can be removed with the incorporation of a spin-3/2 projector in the definitions of the interpolating fields

$$\mathcal{J}^\mu_{X_{3/2}} = P^{\mu\nu}_{3/2} \mathcal{J}_{\nu X}. \tag{16}$$

For nonzero momentum, $P^{\mu\nu}_{3/2}$ is defined by [37]

$$P^{\mu\nu}_{3/2} = \delta^{\mu\nu} - \frac{1}{3}\gamma^\mu\gamma^\nu - \frac{1}{3p^2}(\not{p}\gamma^\mu p^\nu + p^\mu\gamma^\nu\not{p}). \tag{17}$$

In correspondence, the spin-1/2 component $\mathcal{J}^\mu_{X_{1/2}}$ can be obtained by acting with the spin-1/2 projector $P^{\mu\nu}_{1/2} = \delta^{\mu\nu} - P^{\mu\nu}_{3/2}$ on $\mathcal{J}^\mu_X$. Elements with Lorentz indices $\mu, \nu = 0$ will not contribute. In this work we study the mass spectrum of the baryons in the rest frame taking $\vec{p} = \vec{0}$.

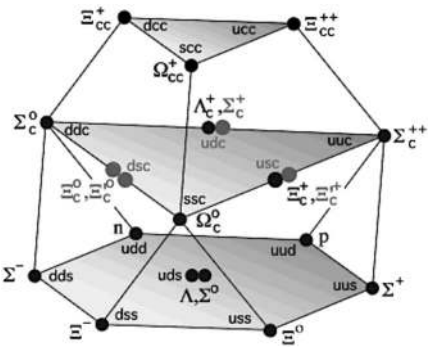

FIG. 2. The 20′-plet of spin-1/2 baryons classified according to their charm content. The lowest level represents the $c = 0$ SU(3) octet.

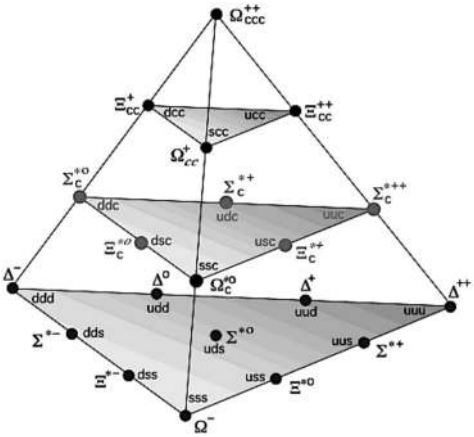

FIG. 3. The 20-plet of spin-3/2 baryons classified according to their charm content. The lowest level represents the $c = 0$ decuplet subgroup.

TABLE II. Smearing parameters for the ensembles at $\beta = 1.90$, $\beta = 1.95$ and $\beta = 2.10$.

		APE		Gaussian	
	$a\mu_l, L/a$	n	α	n	α
$\beta = 1.90$	0.0030, 32	20	0.5	50	4.0
	0.0040, 32	20	0.5	50	4.0
	0.0050, 32	20	0.5	50	4.0
$\beta = 1.95$	0.0025, 32	20	0.5	50	4.0
	0.0035, 32	20	0.5	50	4.0
	0.0055, 32	20	0.5	50	4.0
	0.0075, 32	20	0.5	50	4.0
$\beta = 2.10$	0.0015, 48	50	0.5	110	4.0
	0.0020, 48	20	0.5	50	4.0
	0.0030, 48	20	0.5	50	4.0

Since in that case the last term of Eq. (17) will contain $\delta_{0\mu}$, it will vanish. When the spin-3/2 and spin-1/2 projectors are applied to the interpolating field operators, the resulting two-point correlators for the spin-3/2 baryons acquire the form

$$C_{\frac{3}{2}}(t) = \frac{1}{3}\mathrm{Tr}[C(t)] + \frac{1}{6}\sum_{i\neq j}^{3}\gamma_i\gamma_j C_{ij}(t),$$
$$C_{\frac{1}{2}}(t) = \frac{1}{3}\mathrm{Tr}[C(t)] - \frac{1}{3}\sum_{i\neq j}^{3}\gamma_i\gamma_j C_{ij}(t), \qquad (18)$$

where $\mathrm{Tr}[C] = \sum_i C_{ii}$. When no projector is taken into account, the resulting two-point correlator would be $C = \frac{1}{3}\mathrm{Tr}[C]$.

We have carried out an analysis to examine the results of the effective masses extracted from correlation functions with and without the spin-3/2 projection, as well as with the spin-1/2 projector using 100 gauge configurations, a number sufficiently large for the purpose of this comparison. In our comparison we also consider correlation functions obtained using the alternative interpolating fields given in Table XIV. To distinguish these two sets we denote the interpolating fields of Tables XII and XIII by $\mathcal{J}_B$ and those in Table XIV by $\tilde{\mathcal{J}}_B$. The left panel of Fig. 4 compares effective masses extracted from correlators with $\mathcal{J}_{\Sigma^{*+}}$ at $\beta = 2.10$, $a\mu_l = 0.0015$. As can be seen, the results for the effective masses when applying the 3/2-projector and without any projection are perfectly consistent even at short source-sink time separations yielding the mass of Σ^{*+}. On the other hand, the effective mass obtained using the spin-1/2 projected interpolating field is much more noisy and yields a higher value of the mass. The latter property suggests that the 1/2-projected interpolating field $\mathcal{J}_{\Sigma^*}$ yields an excited spin-1/2 state of the Σ^* at least at small time slices. The large errors associated with the correlator with the spin-1/2 projector suggest that the overlap with this state is weak. Another example is shown in the right panel of Fig. 4, where results are displayed for the correlator using $\mathcal{J}_{\Sigma_c^{*++}}$ at $\beta = 1.95$, $a\mu_l = 0.0055$. A similar behavior to ours for the Σ_c^{*++} was found in Ref. [38] where the same spin projections are implemented. However, there are cases where the spin-3/2 projection is required. One example is the Ξ^{*-} baryon, shown in Fig. 5, where the effective mass when no projection is applied is persistently lower than when using the spin-3/2 projector. It is also apparent from Fig. 5 that the spin-1/2 projected interpolating field $\mathcal{J}_{\Xi^{*-}}$ yields an effective mass, which is consistent with the corresponding results using the spin-1/2 interpolating field $\mathcal{J}_{\Xi^-}$ and thus the mass of Ξ^-. A similar case to this is the Ξ^{*0}, as can be seen from Fig. 6. Therefore, it is crucial in order to obtain the correct spin-3/2 mass to project out the lower-lying spin-1/2 state.

In order to further examine the properties of the interpolating fields, we also include effective mass results from the alternative set of interpolating fields. We plot effective mass results obtained from $\tilde{\mathcal{J}}_{\Xi^{*0}}$ as well as the effective mass of the spin-1/2 Ξ^0 at $\beta = 1.95$,

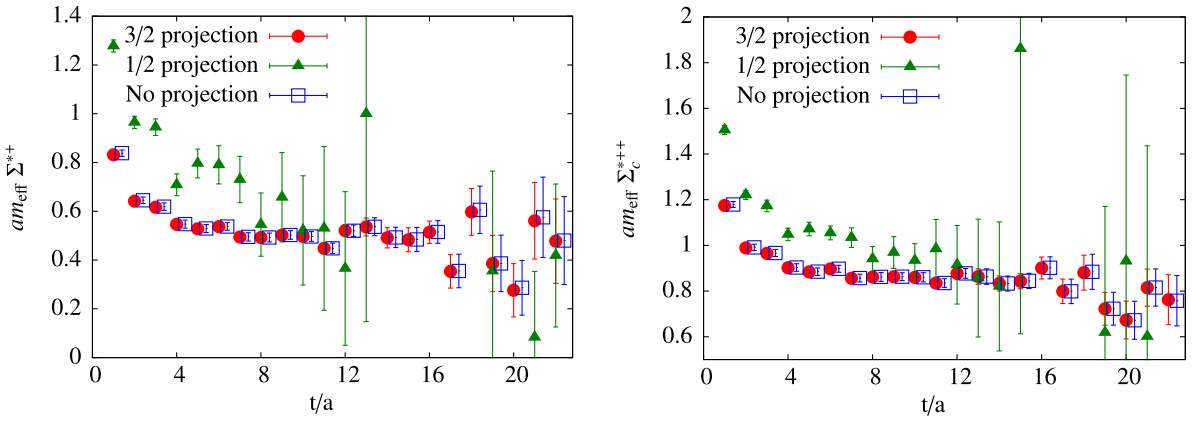

FIG. 4 (color online). Comparison of effective masses extracted using $\mathcal{J}_{\Sigma^{*+}}$ at $\beta = 2.10$, $a\mu_l = 0.0015$ (left) and using $\mathcal{J}_{\Sigma_c^{*++}}$ at $\beta = 1.95$, $a\mu_l = 0.0055$ (right) obtained with the spin-3/2 projection (red filled circles), spin-1/2 projection (green triangles) and without projection (blue open squares, shifted to the right for clarity).

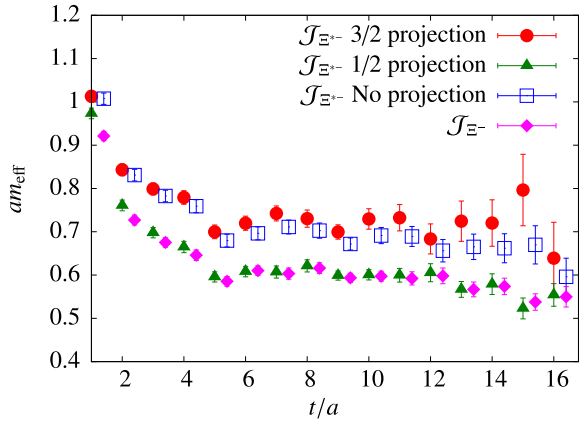

FIG. 5 (color online). Comparison of effective masses extracted using for $\mathcal{J}_{\Xi^{*-}}$ at $\beta = 1.95$, $a\mu_l = 0.0025$ obtained with the spin-3/2 projection (red filled circles), without projection (blue open squares, shifted to the right for clarity) and with spin-1/2 projection (green triangles). Also plotted is the effective mass using $\mathcal{J}_{\Xi^-}$ (magenta diamonds).

$a\mu_l = 0.0025$ in Fig. 7, in correspondence with Fig. 6. As shown, the results from using spin-3/2 projection and when applying no projection on $\tilde{\mathcal{J}}_{\Xi^{*0}}$ are now consistent. In contrast with $\mathcal{J}_{\Xi^{*0}}$, the spin-1/2 projection of $\tilde{\mathcal{J}}_{\Xi^{*0}}$ yields an excited spin-1/2 state of Ξ^{*0}. However, as can be seen from Fig. 8, the spin-3/2 projections of the two interpolating fields for Ξ^{*0} yield fully consistent results, as expected. Similar behavior is observed in the other baryon states as well. We demonstrate this by showing results for Ω_c^{*0} at $\beta = 1.95$, $a\mu_l = 0.0075$ in Figs. 9 and 10.

The main conclusion of this analysis is that the set of spin-3/2 $\tilde{\mathcal{J}}$ interpolating fields do not need any spin-3/2 projection, whereas the $\mathcal{J}$ in general do. After spin-3/2 projection they both give consistent results for the mass of the spin-3/2 state they represent, as expected. Therefore from now on we use only results from spin-3/2 projected

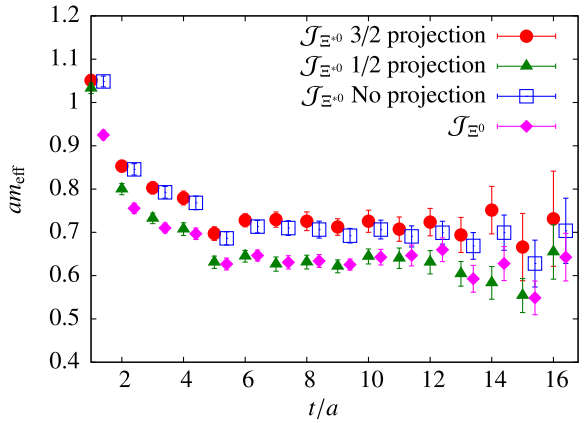

FIG. 6 (color online). Comparison of effective masses for Ξ^{*0} at $\beta = 1.95$, $a\mu_l = 0.0025$ obtained with the spin-3/2 projection, without projection and with spin-1/2 projection. Also plotted is the effective mass of Ξ^0. The notation is as in Fig. 5.

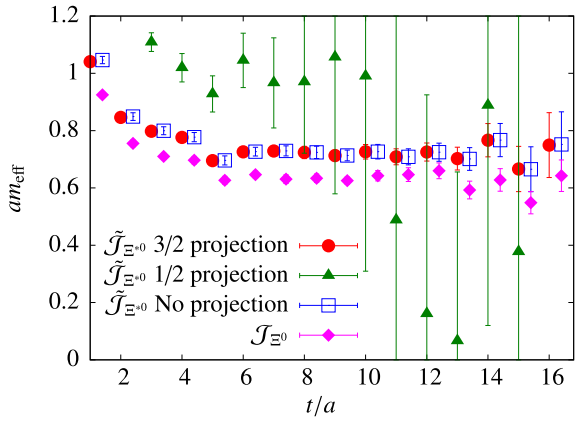

FIG. 7 (color online). Effective masses obtained using $\tilde{\mathcal{J}}_{\Xi^{*0}}$ at $\beta = 1.95$, $a\mu_l = 0.0025$ with the spin-3/2 projection (red filled circles), without projection (blue open squares, shifted to the right for clarity) and with spin-1/2 projection (green triangles). Also plotted is the effective masses using $\tilde{\mathcal{J}}_{\Xi^0}$ (magenta diamonds).

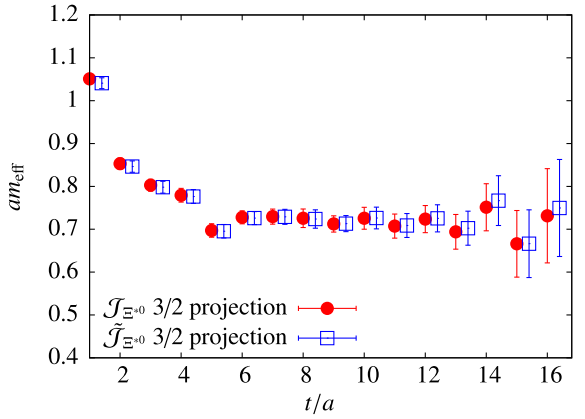

FIG. 8 (color online). Comparison of effective masses for Ξ^{*0} at $\beta = 1.95$, $a\mu_l = 0.0025$ obtained from $\mathcal{J}_{\Xi^{*0}}$ (red filled circles) and $\tilde{\mathcal{J}}_{\Xi^{*0}}$ (blue open squares, shifted to the right for clarity) using the spin-3/2 projection. Results from the two interpolating fields are fully consistent.

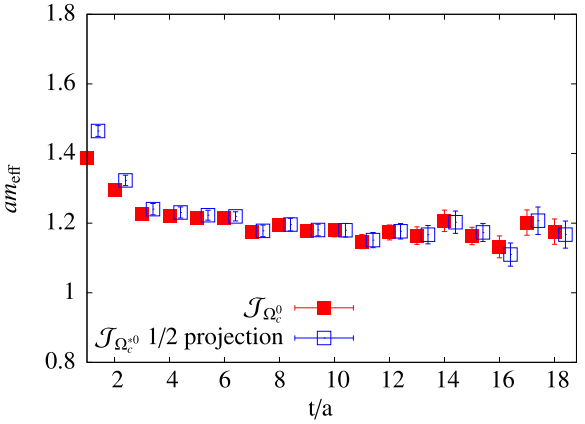

FIG. 9 (color online). Effective mass results obtained for Ω_c^0 (red filled squares) and from $\mathcal{J}_{\Omega_c^{*0}}$ using the spin-1/2 projection (blue open squares). The results are in agreement.

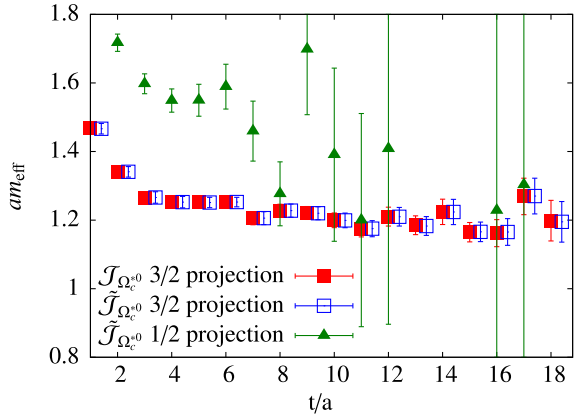

FIG. 10 (color online). Effective mass results of Ω_c^{*0} obtained from the spin-3/2 projections of $\mathcal{J}_{\Omega_c^{*0}}$ (red filled squares) and $\tilde{\mathcal{J}}_{\Omega_c^{*0}}$ (blue open squares) as well as from the spin-1/2 projection of $\tilde{\mathcal{J}}_{\Omega_c^{*0}}$ (green triangles). More details are given in the text.

interpolating fields and limit ourselves to the interpolating fields $\mathcal{J}$ listed in Tables XII and XIII.

E. Determination of the lattice spacing

Since in this work the observables discussed are the masses of baryons, the physical nucleon mass is the most appropriate quantity to set the scale. In order to determine the values of the lattice spacings as accurate as possible we have carried out a high statistics analysis of the nucleon masses for a total of 17 $N_f = 2 + 1 + 1$ gauge ensembles at $\beta = 1.90$, $\beta = 1.95$ and $\beta = 2.10$ on a range of pion masses and volumes. We average over the masses of the proton and neutron to further gain on statistics. The resulting nucleon masses for each of the gauge ensembles are collected in Table III.

The nucleon masses as function of m_π^2 are presented in Fig. 11. As can be seen, cutoff effects are negligible, therefore we can use continuum chiral perturbation theory to extrapolate to the physical pion mass using all the lattice results. To this end we consider SU(2) chiral perturbation theory (χPT) [39] and the well-established $\mathcal{O}(p^3)$ result of the nucleon mass dependence on the pion mass, given by

$$m_N = m_N^{(0)} - 4c_1 m_\pi^2 - \frac{3g_A^2}{32\pi f_\pi^2} m_\pi^3 \tag{19}$$

where m_N^0 is the nucleon mass at the chiral limit and together with c_1 are treated as fit parameters. This lowest order result for the nucleon in heavy baryon chiral perturbation theory (HBχPT), first derived in Ref. [40], and describes well lattice data [13,41]. Since this result is well established as the leading contribution irrespective of the various approaches to compute higher orders such as in HBχPT with dimensional and infra-red regularization with and without the Δ degree of freedom explicitly included, we will use it to fix the lattice spacing from the nucleon mass The lattice spacings $a_{\beta=1.90}$, $a_{\beta=1.95}$ and $a_{\beta=2.10}$ are considered as additional independent fit parameters in a combined fit of our data at $\beta = 1.90$, $\beta = 1.95$ and $\beta = 2.10$. We constrain our fit so that the fitted curve passes through the physical point by fixing the value of c_1. The physical values of f_π and g_A are used in the fits, namely $f_\pi = 0.092419(7)(25)$ GeV and $g_A = 1.2695(29)$, which is common practice in chiral fits to lattice data on the nucleon mass [42–44]. The left panel of Fig. 11 shows the

TABLE III. Values of the nucleon masses with the associated statistical error.

Volume	Statistics	$a\mu_l$	am_π	m_π (GeV)	am_N	m_N (GeV)
			$\beta = 1.90$			
	740	0.0030	0.1240	0.2607	0.5239(87)	1.1020(183)
$32^3 \times 64$	1556	0.0040	0.1414	0.2975	0.5192(112)	1.0921(235)
	387	0.0050	0.1580	0.3323	0.5422(62)	1.1407(130)
	2092	0.0400	0.1449	0.3049	0.5414(84)	1.1389(176)
	1916	0.0060	0.1728	0.3634	0.5722(48)	1.2036(101)
$24^3 \times 48$	1796	0.0080	0.1988	0.4181	0.5898(50)	1.2407(104)
	2004	0.0100	0.2229	0.4690	0.6206(43)	1.3056(90)
$20^3 \times 48$	617	0.0040	0.1493	0.3140	0.5499(195)	1.1568(410)
			$\beta = 1.95$			
	2892	0.0025	0.1068	0.2558	0.4470(59)	1.0706(141)
	4204	0.0035	0.1260	0.3018	0.4784(48)	1.1458(114)
$32^3 \times 64$	18576	0.0055	0.1552	0.3716	0.5031(16)	1.2049(39)
	2084	0.0075	0.1802	0.4316	0.5330(42)	1.2764(100)
$24^3 \times 48$	937	0.0085	0.1940	0.4645	0.5416(50)	1.2970(121)
			$\beta = 2.10$			
	2424	0.0015	0.0698	0.2128	0.3380(41)	1.0310(125)
$48^3 \times 96$	744	0.0020	0.0805	0.2455	0.3514(70)	1.0721(215)
	226	0.0030	0.0978	0.2984	0.3618(68)	1.1038(208)
$32^3 \times 64$	1905	0.0045	0.1209	0.3687	0.3944(26)	1.2032(79)

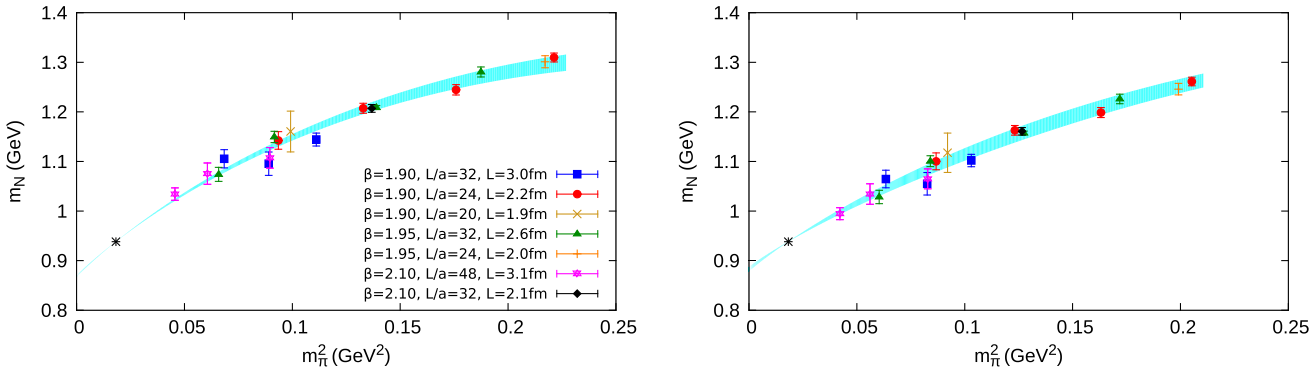

FIG. 11 (color online). Nucleon masses at the three values of the lattice spacing. On the left panel the solid band represents a fit to the lowest order $\mathcal{O}(p^3)$ expansion from HBχPT. The band on the right panel is a fit to $\mathcal{O}(p^4)$ with explicit Δ degrees of freedom in the so-called SSE. The physical nucleon mass is denoted with the asterisk.

fit to the $\mathcal{O}(p^3)$ result of Eq. (19) on the nucleon mass. The error band and the errors on the fit parameters are obtained from super-jackknife analysis [45]. As can be seen, the $\mathcal{O}(p^3)$ result provides a very good fit to our lattice data, which in fact confirms that cutoff and finite volume effects are small for the β values used. In addition, our lattice results exhibit a curvature which supports the presence of the m_π^3-term.

In order to estimate the systematic error due to the chiral extrapolation we also perform a fit using HBχPT to $\mathcal{O}(p^4)$ in the so-called small scale expansion (SSE) [44]. This form includes explicit Δ degrees of freedom by introducing as an additional parameter the Δ-nucleon mass splitting, $\Delta \equiv m_\Delta - m_N$, taking $\mathcal{O}(\Delta/m_N) \sim \mathcal{O}(m_\pi/m_N)$. In SSE the nucleon mass is given by

$$\begin{aligned} m_N = {} & m_N^0 - 4c_1 m_\pi^2 - \frac{3g_A^2}{32\pi f_\pi^2} m_\pi^3 - 4E_1(\lambda) m_\pi^4 \\ & - \frac{3(g_A^2+3c_A^2)}{64\pi^2 f_\pi^2 m_N^0} m_\pi^4 - \frac{(3g_A^2+10c_A^2)}{32\pi^2 f_\pi^2 m_N^0} m_\pi^4 \log\left(\frac{m_\pi}{\lambda}\right) \\ & - \frac{c_A^2}{3\pi^2 f_\pi^2}\left(1+\frac{\Delta}{2m_N^0}\right)\left[\frac{\Delta}{4} m_\pi^2 + \left(\Delta^3 - \frac{3}{2} m_\pi^2 \Delta\right)\log\left(\frac{m_\pi}{2\Delta}\right) \right. \\ & \left. + (\Delta^2 - m_\pi^2) R(m_\pi)\right] \end{aligned} \tag{20}$$

where $R(m_\pi) = -\sqrt{m_\pi^2 - \Delta^2}\cos^{-1}(\frac{\Delta}{m_\pi})$ for $m_\pi > \Delta$ and $R(m_\pi) = \sqrt{\Delta^2 - m_\pi^2}\log(\frac{\Delta}{m_\pi} + \sqrt{\frac{\Delta^2}{m_\pi^2} - 1})$ for $m_\pi < \Delta$. We take the cutoff scale $\lambda = 1$ GeV, $c_1 = 1.127$ [44] and treat the counterterm E_1 as an additional fit parameter. As in the $\mathcal{O}(p^3)$ case we use the physical values of g_A and f_π. The corresponding plot is shown on the right panel of Fig. 11. The error band as well as the errors on the fit parameters are obtained using super-jackknife analysis. One can see that this formulation provides a good description of the lattice data as well and yields values of the lattice spacings and m_N^0 which are consistent with those obtained in $\mathcal{O}(p^3)$ of HBχPT. We take the difference between the results of the $\mathcal{O}(p^3)$ and $\mathcal{O}(p^4)$ fits as an estimate of the uncertainty due to the chiral extrapolation. This is found to be about three times the statistical error. The final values of the lattice spacing are shown in Eq. (21). The first parenthesis is the statistical error and the systematic error is given is the second parenthesis. The rest of the fit parameters for the two expansions and the χ^2/d.o.f. are given in Table IV.

$$\begin{aligned} a_{\beta=1.90} &= 0.0936(13)(35)\ \text{fm}, \\ a_{\beta=1.95} &= 0.0823(10)(35)\ \text{fm}, \\ a_{\beta=2.10} &= 0.0646(7)(25)\ \text{fm}. \end{aligned} \tag{21}$$

In order to better assess discretization effects we perform a fit to $\mathcal{O}(p^3)$ at each of the β values separately. The values we find are $a_{\beta=1.90} = 0.0923(20)$ fm, $a_{\beta=1.95} = 0.0821(16)$ fm and $a_{\beta=2.10} = 0.0657(12)$ fm. These values are fully consistent with those obtained in Eq. (21) from the combined fit, indicating that discretization effects are small, thus confirming *a posteriori* the validity of the assumption that cutoff effects are small for the nucleon

TABLE IV. Fit parameters m_N^0 in GeV and $E_1(\lambda)$ in GeV^{-3} from $\mathcal{O}(p^3)$ χPT and $\mathcal{O}(p^4)$ SSE, as well as the fixed value of $-4c_1$. Also included is the value of the σ-term for each fit.

	m_N^0	$-4c_1$(GeV^{-1})	$E_1(\lambda)$ (GeV^{-3})	$\sigma_{\pi N}$ (MeV)	χ^2/d.o.f.
$\mathcal{O}(p^3)$ HBχPT	0.8667(15)	4.5735		64.9(1.5)	1.5779
$\mathcal{O}(p^4)$ SSE	0.8813(47)	3.7282	−2.5858(2480)	45.3(4.3)	1.0880

mass. A different way of demonstrating this is to include a quadratic term da^2 to Eqs. (19) and (20), treating d as an additional fit parameter. Performing the fits with the da^2-term gives a value of $d = 0.017(17)$ GeV^3 i.e. consistent with zero. The same is true for the Δ mass confirming that cutoff effects are negligible in the light quark sector.

We will use the values given in Eq. (21) to convert to physical units all the quantities studied in this work. We note that when performing these fits only statistical errors are taken into account and systematic errors due to the choice of the plateau are not included. The lattice spacings for these β values were also calculated from a pion decay constant analysis using next-to-leading order (NLO) SU(2) chiral perturbation theory for the extrapolations [46]. In that preliminary analysis only a subset of the ensembles used here was included, yielding values of the lattice spacings that are smaller compared to the values we extract using the nucleon mass in this work. Specifically, the lattice spacings at $\beta = 1.90, 1.95$ and 2.10 were found to be $a_{f_\pi} = 0.0863(4), 0.0779(4)$ and $0.607(2)$ respectively, where a_{f_π} denotes the lattice spacing determined using the pion decay constant. This implies that the values of the pion masses in physical units we quote in this paper are equivalently smaller than those obtained using f_π to convert to physical units. A comprehensive study of the different lattice spacing determinations is ongoing.

Having determined the parameters of the chiral fit we can compute the nucleon $\sigma_{\pi N}$-term by evaluating $m_\pi^2 \partial m_N / \partial m_\pi^2$ where we have taken the leading order relation $m_\pi^2 \sim \mu_l$. Using Eq. (19) we find $\sigma_{\pi N} = 64.9 \pm 1.5$ MeV. This value is fully consistent with previous values extracted using this lowest order fit by ETMC on $N_f = 2$ quark flavor ensembles [13,41]. Performing the same calculation using the $\mathcal{O}(p^4)$ expression we obtain a lower value of $\sigma_{\pi N} = 45.3 \pm 4.3$ MeV showing the sensitivity to the chiral extrapolation. It is worth mentioning that such a difference in the determination of the $\sigma_{\pi N}$-term is known in the literature. For example, a latest πN scattering study [47], reporting a value $\sigma_{\pi N} = 59 \pm 7$ MeV, while higher values were also obtained using the Feynman-Hellmann theorem to analyze lattice QCD data yielding $\sigma_{\pi N} = 55 \pm 1$ MeV [48]. Lower values are associated with the well-known result of $\sigma_{\pi N} = 45 \pm 8$ MeV extracted from an earlier chiral perturbation analysis of experimental scattering data [49], as well as, with the values extracted in other lattice QCD calculations, such as the analysis of the QCDSF Collaboration [50], where a value $\sigma_{\pi N} = 38 \pm 12$ MeV is obtained and of Ref. [51] where a value of $\sigma_{\pi N} = 52 \pm 3 \pm 8$ is extracted from a flavor SU(2) extrapolation of a large set of lattice data on the nucleon mass. A very recent result is obtained using the relativistic chiral Lagrangian from Ref. [52], suggests a rather smaller value of $\sigma_{\pi N} = 39 + 2 - 1$ MeV. We summarize lattice results on $\sigma_{\pi N}$ in Fig. 12 we show our $\mathcal{O}(p^3)$ value. We take difference between the value extracted from the $\mathcal{O}(p^4)$ expression of Eq. (20) and the $\mathcal{O}(p^3)$ value as an estimate for the error arising from chiral extrapolation. As can be seen from the values in Table IV the chiral extrapolation error is large showing the sensitivity on the chiral extrapolation, which explains the large error shown on our $\sigma_{\pi N}$ results. It is apparent that, despite the long efforts, the precise determination of the nucleon σ-terms is still an open issue and direct techniques as those described in for example Ref. [53] are welcome.

F. Tuning of the bare strange and charm quark masses

A tuning of the bare strange and charm quark masses is performed using the physical mass of the Ω^- and the Λ_c^+ baryons respectively. For the tuning we calculate the Ω^-

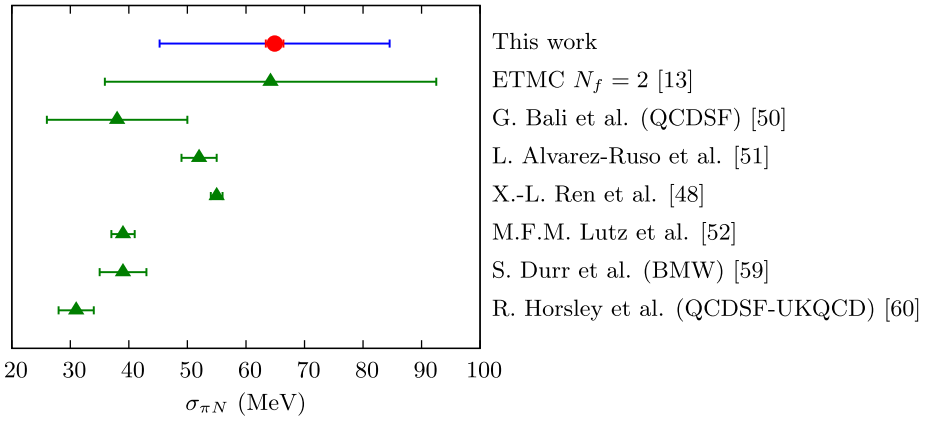

FIG. 12 (color online). Comparison of lattice results for $\sigma_{\pi N}$ in MeV, extracted from the $\mathcal{O}(p^3)$ analysis of this work with the results from other lattice calculations. Our result shows the statistical error in red and a systematic error in blue taken as the difference between the value obtained using the $\mathcal{O}(p^3)$ and $\mathcal{O}(p^4)$ expressions [Eqs. (19) and (20) respectively] providing an estimate of the uncertainty due to the chiral extrapolation.

and Λ_c^+ masses at a given value of the renormalized strange and charm quark mass for all β values. For this we need the renormalization constants Z_P for the three β values. These were computed in Ref. [54] and we quote, for the convenience of the reader, the values computed in the $\overline{\text{MS}}$ scheme at 2 GeV:

$$Z_P^{\beta=1.90} = 0.529(7),$$
$$Z_P^{\beta=1.95} = 0.509(4),$$
$$Z_P^{\beta=2.10} = 0.516(2). \quad (22)$$

For the Ω^- we use the leading one-loop result from SU(2) χPT, given by

$$m_\Omega = m_\Omega^{(0)} - 4c_\Omega^{(1)} m_\pi^2, \quad (23)$$

where the mass $m_\Omega^{(0)}$ and $c_\Omega^{(1)}$ are treated as fit parameters. For the Λ_c^+ baryon, we use the result motivated by SU(2) HBχPT to leading one-loop order given by

$$m_{\Lambda_c} = m_{\Lambda_c}^{(0)} + c_1 m_\pi^2 + c_2 m_\pi^3, \quad (24)$$

where $m_{\Lambda_c}^{(0)}$ and the coefficients c_i are treated as fit parameters. We include cutoff effects, by adding a quadratic term da^2 to the Eqs. (23) and (24), where d is treated as an additional fit parameter. The fit then yields the result at the physical point in the continuum limit. We use the lattice spacings given in Eq. (21) extracted from the nucleon mass to convert the Ω^- and Λ_c masses to physical units.

In order to perform the tuning we use several values of the strange and charm quark masses for the gauge ensembles considered in this work, as listed in Table V. Our strategy is to interpolate the Ω^- and Λ_c^+ masses to a given value of the renormalized strange and charm quark mass, respectively, and then extrapolate to the physical point using Eqs. (23) and (24) to compare with the experimental values. The value of the renormalized quark mass is then changed iteratively until the extrapolated continuum values

TABLE V. The values of the strange and charm quark masses for each ensemble used for the tuning.

Ensemble		am_s	m_s^R (GeV)	am_c	m_c^R (GeV)
$\beta = 1.90$	$a\mu_l = 0.0030, L/a = 32$	0.0229	0.0904	0.2968	1.1737
		0.0234	0.0924	0.2999	1.1860
	$a\mu_l = 0.0040, L/a = 32$	0.0232	0.0917	0.2851	1.1272
		0.0234	0.0924	0.2999	1.1860
		0.0264	0.1043		
	$a\mu_l = 0.0050, L/a = 32$	0.0234	0.0924	0.2943	1.1637
				0.2999	1.1860
$\beta = 1.95$	$a\mu_l = 0.0025, L/a = 32$	0.0182	0.0862	0.2350	1.1122
		0.0192	0.0909	0.2506	1.1860
		0.0195	0.0924	0.2550	1.2069
		0.0200	0.0947	0.2694	1.2752
	$a\mu_l = 0.0035, L/a = 32$	0.0187	0.0883	0.2250	1.0649
		0.0195	0.0924	0.2450	1.1596
		0.0200	0.0970	0.2506	1.1860
				0.2580	1.2210
	$a\mu_l = 0.0055, L/a = 32$	0.0186	0.0879	0.2350	1.1122
		0.0195	0.0924	0.2506	1.1860
		0.0200	0.0970	0.2570	1.2164
				0.2715	1.2848
	$a\mu_l = 0.0075, L/a = 32$	0.0195	0.0924	0.2240	1.0602
		0.0200	0.0970	0.2440	1.1548
				0.2506	1.1860
$\beta = 2.10$	$a\mu_l = 0.0015, L/a = 48$	0.0155	0.0919	0.1850	1.0959
		0.0156	0.0924	0.2000	1.1847
		0.0162	0.0959	0.2002	1.1860
		0.0169	0.1002	0.2195	1.3002
	$a\mu_l = 0.0020, L/a = 48$	0.0156	0.0924	0.1900	1.1255
		0.0158	0.0936	0.2002	1.1860
		0.0165	0.0977	0.2150	1.2736
	$a\mu_l = 0.0030, L/a = 48$	0.0156	0.0924	0.1800	1.0662
		0.0163	0.0965	0.2002	1.1860
				0.2080	1.2321

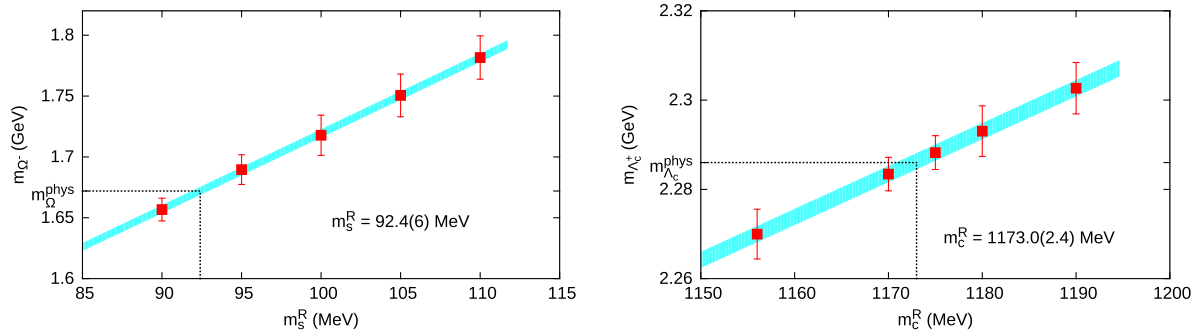

FIG. 13 (color online). Tuning of the renormalized strange and charm quark masses with the experimental values of the Ω (left) and Λ_c^+ (right) masses respectively.

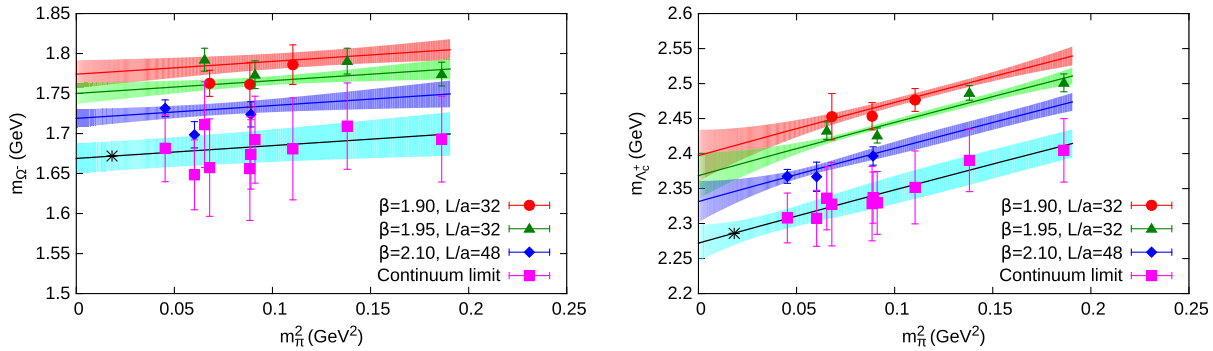

FIG. 14 (color online). Chiral extrapolations of the lattice data for Ω^- (left) and Λ_c (right) at the fixed values of the renormalized strange and charm quark masses of Eq. (25) respectively. In these figures, the lattice data for each β value as well as the continuum extrapolated values are plotted. The physical masses of Ω^- and Λ_c are reproduced at the continuum limit and at the physical pion mass.

agree with the experimental ones. This determines the tuned values of m_s^R and m_c^R that reproduce the physical masses of Ω^- and Λ_c^+, respectively. In Fig. 13 we show representative plots from the determination of m_S^R and m_c^R. We obtain the following values in $\overline{\text{MS}}$ at 2 GeV:

$$m_s^R = 92.4(6)(2.0)\ \text{MeV}$$
$$m_c^R = 1173.0(2.4)(17.0)\ \text{MeV}. \quad (25)$$

The error in the first parenthesis is the statistical error on the fit parameters and in the second parenthesis is the error associated with the tuning estimated by allowing the renormalized mass to vary within the statistical errors of the Ω^- and Λ_c^+ mass at the physical point. The latter systematic uncertainty due to the tuning will be included in the final errors we quote for the baryon masses. In Ref. [54] the mass of the kaon and D-meson were used to tune the strange and charm quark masses, obtaining $m_s^R = 99.6(4.1)$ MeV and $m_c^R = 1176(36)$ MeV in $\overline{\text{MS}}$ at 2 GeV, respectively, both in agreement with our values. The corresponding plots of the chiral extrapolations for Ω^- (Λ_c^+) at the fixed value of the strange (charm) quark mass after correcting for cutoff effects are shown in Fig. 14, where indeed all data fall on the same curve and the physical masses of the Ω^- and Λ_c^+ baryons are reproduced. The fit parameters $m_\Omega^{(0)}$, $c_\Omega^{(1)}$ and c_i are collected in Table VII. The results in lattice units and the continuum extrapolated values in physical units for Ω^- and Λ_c^+ are listed in Table VI.

Given the fact that we have performed a high statistics run (see Table I) using $m_c^R = 1186$ MeV, which was our first estimate for m_c^R and since this value is consistent with

TABLE VI. Masses of the Ω and Λ_c^+ baryons in lattice and physical units with the associated statistical error. The values in physical units are continuum extrapolated.

$a\mu_l$	am_Ω	m_Ω (GeV)	$am_{\Lambda_c^+}$	$m_{\Lambda_c^+}$ (GeV)
		$\beta = 1.90$		
0.0030	0.8380(77)	1.6575(609)	1.1651(157)	2.3223(729)
0.0040	0.8374(131)	1.6562(648)	1.1714(92)	2.3356(678)
0.0050	0.8491(118)	1.6808(637)	1.1816(78)	2.3571(670)
		$\beta = 1.95$		
0.0025	0.7484(60)	1.7111(535)	1.0236(52)	2.3523(584)
0.0035	0.7406(72)	1.6924(544)	1.0261(45)	2.3581(581)
0.0055	0.7477(67)	1.7093(540)	1.0434(43)	2.3997(580)
0.0075	0.7409(62)	1.6931(536)	1.0468(53)	2.4077(585)
		$\beta = 2.10$		
0.0015	0.5676(34)	1.6816(418)	0.7817(33)	2.3234(459)
0.0020	0.5568(54)	1.6484(437)	0.7796(68)	2.3171(494)
0.0030	0.5651(51)	1.6740(434)	0.7883(43)	2.3438(467)

TABLE VII. Fit parameters and physical point values determined from the chiral fits to the Ω^- and Λ_c^+ using Eqs. (23) and (24) respectively.

Ω^- (1.672)	
$m_\Omega^{(0)}$ (GeV)	1.669(19)
$-4c_\Omega^{(1)}$ (GeV^{-1})	0.161(124)
d (GeV^3)	0.466(123)
χ^2/d.o.f.	2.24
m (GeV)	1.672(18)
Λ_c^+ (2.286)	
$m_{\Lambda_c}^{(0)}$ (GeV)	2.272(26)
c_1 (GeV^{-1})	0.799(935)
c_2 (GeV^{-2})	−0.118(1.834)
d (GeV^3)	0.553(104)
χ^2/d.o.f.	1.33
m (GeV)	2.286(17)

the final tuned value given in Eq. (25) we will use the high statistics results to obtain the values of the charmed-baryon masses at the physical point. We have checked that interpolation of our lattice data for the charm baryons at the tuned value of $m_c^R = 1173(2.4)$ yield masses at the physical point which are totally consistent with the ones obtained at $m_c^R = 1186(2.4)$, albeit with larger errors due to the interpolation of the lattice results. Thus, we avoid interpolation and use the results obtained directly at $m_c^R = 1186$ MeV in what follows.

III. LATTICE RESULTS

Lattice results are obtained for three lattice spacings allowing to assess cutoff effects. We start by addressing any possible isospin breaking effects on the baryon masses.

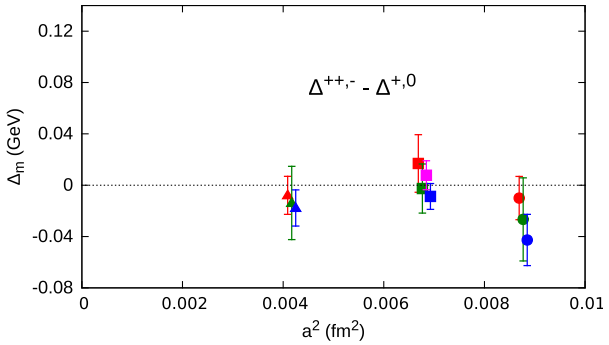

FIG. 15 (color online). Mass differences for the Δ baryons for our three lattice spacings (circles for $\beta = 1.90$, squares for $\beta = 1.95$ and triangles for $\beta = 2.10$) examined and for all pion masses. Symbols for each lattice spacing have been shifted to the left and right for clarity. Red symbols represent the lightest pion mass and blue symbols the heaviest pion mass for each lattice spacing. For $\beta = 1.95$, the green symbol is the second lightest pion mass and the magenta symbol is the second heaviest pion mass.

A. Isospin symmetry breaking

The twisted mass action breaks isospin explicitly to $\mathcal{O}(a^2)$ and the size of the $\mathcal{O}(a^2)$-terms determines how large this breaking is. Any isospin splitting should vanish in the continuum limit. In general, isospin symmetry breaking manifests itself as a mass splitting among baryons belonging to the same multiplets. We note that there is still a symmetry when interchanging a u- with a d-quark, which means for example that the proton and the neutron are still degenerate as are the Δ^{++} and the Δ^- as well as the Δ^+ and Δ^0. However, mass splitting could be seen between the

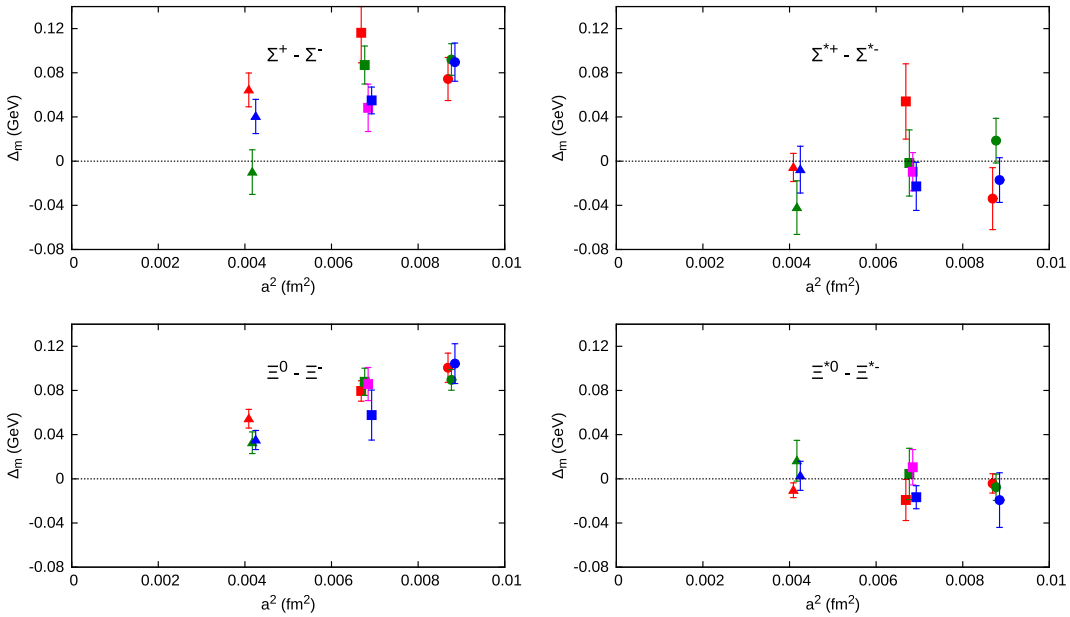

FIG. 16 (color online). Mass differences for the octet (left) and decuplet (right) hyperons for our three lattice spacings examined. Small nonzero mass differences are observed for the octet hyperons. The symbol notation is as in Fig. 15.

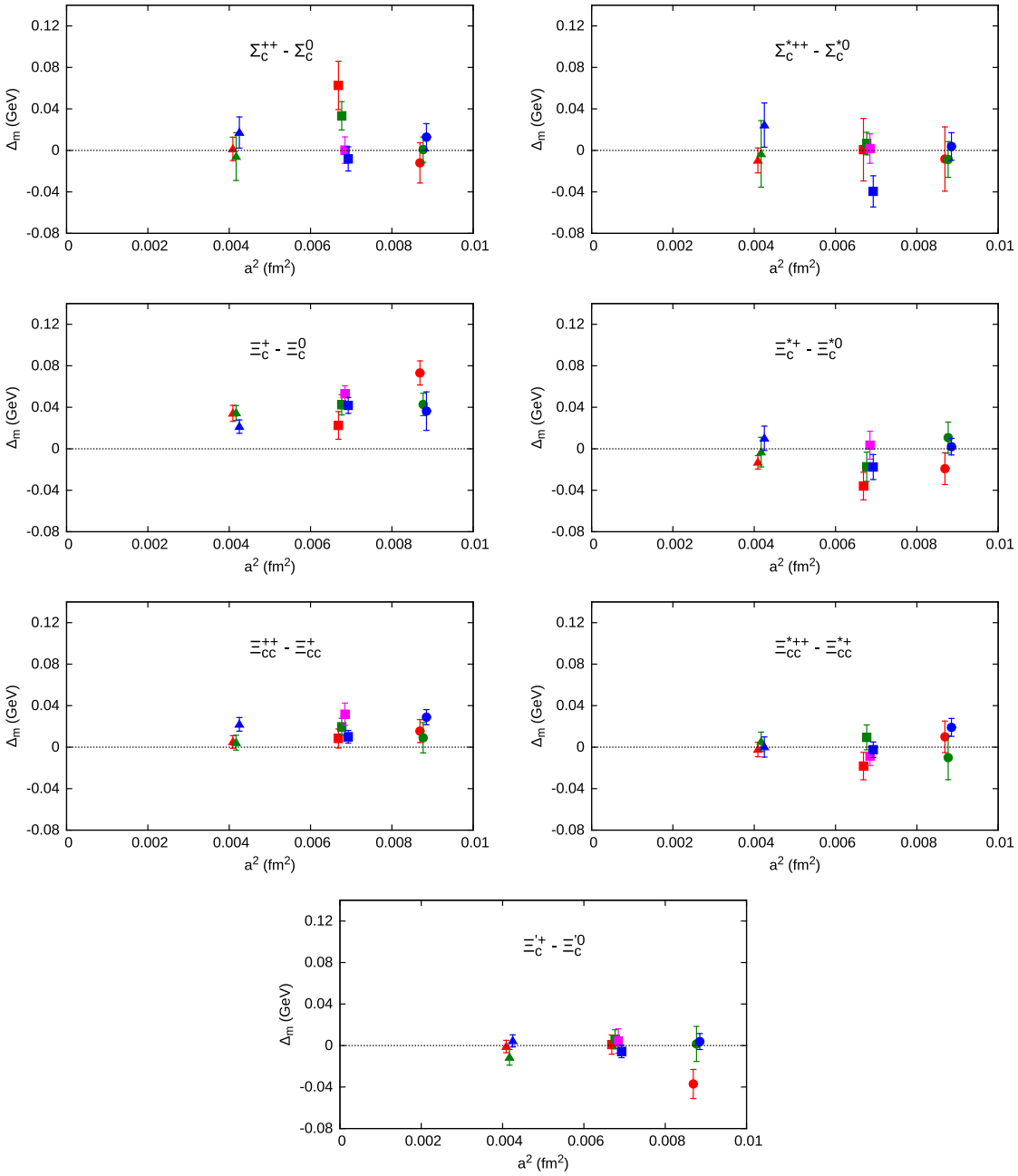

FIG. 17 (color online). Mass differences between the charm baryons belonging to the same isospin multiplets for the three lattice spacings. Small nonzero differences which are reduced as the lattice spacing gets smaller are seen between the Ξ_c states. The notation is the same as that in Fig. 15.

Δ^{++} and the Δ^{+}. Also, isospin breaking effects maybe present in the hyperons and charmed baryons in particular given that we consider only the s^+ and c^+, as explained in Sec. II A.

We begin this analysis by plotting the mass difference as a function of a^2 for the Δ baryons. We average over Δ^{++} and Δ^{-} as well as over Δ^{+} and Δ^{0} and take the difference between the two averages. The corresponding plot is shown in Fig. 15, where as one can see, the mass difference is consistent with zero, indicating that isospin breaking effects are small for the Δ baryons at the β values analyzed. We also examine the mass difference of the strange baryons in Fig. 16. We observe that the mass difference between the Σ^+ and Σ^- and between the Ξ^0 and Ξ^- are indeed decreasing linearly with a^2 being almost zero at our smallest lattice spacing. For the strange spin-3/2 baryons the results are fully consistent with zero at all lattice spacings.

We continue our analysis by studying the isospin breaking for the charm baryons. We show in Fig. 17 the mass difference between the Σ_c, Ξ_c and Ξ_{cc} multiplets at the three lattice spacings for all pion masses considered in this work. As in the strange sector, nonzero values are obtained at the largest lattice spacing, which do not exceed 3% the average mass of these baryons. As expected, the mass splitting vanishes as the continuum limit is approached. In the same figure we also show the mass difference between $\Xi_c'^{+}$ and $\Xi_c'^{0}$, which is consistent with zero indicating that isospin breaking effects are small at all values of the lattice spacing. As in the case of the strange decuplet, the isospin splitting for the charmed spin-3/2 baryons is consistent with zero.

Having several pion masses at a given lattice spacing one can ask how the isospin mass splitting depends on the pion mass. As shown in Figs. 16 and 17, the baryon mass differences are independent of the light quark mass to the present accuracy of our results.

IV. CHIRAL AND CONTINUUM EXTRAPOLATION

In order to extrapolate our lattice results to the physical pion mass we allow for cutoff effects by including a term quadratic in the lattice spacing and then apply continuum chiral perturbation theory at our results.

For the strange baryon sector we consider SU(2) HBχPT. The same expressions were used in other twisted mass fermion studies [13,41,55] and were found to describe lattice data satisfactory. The leading one-loop results for the octet and decuplet baryons [56,57] are given by

$$\begin{aligned} m_\Lambda(m_\pi) &= m_\Lambda^{(0)} - 4c_\Lambda^{(1)} m_\pi^2 - \frac{g_{\Lambda\Sigma}^2}{16\pi f_\pi^2} m_\pi^3 \\ m_\Sigma(m_\pi) &= m_\Sigma^{(0)} - 4c_\Sigma^{(1)} m_\pi^2 - \frac{2g_{\Sigma\Sigma}^2 + g_{\Lambda\Sigma}^2/3}{16\pi f_\pi^2} m_\pi^3 \\ m_\Xi(m_\pi) &= m_\Xi^{(0)} - 4c_\Xi^{(1)} m_\pi^2 - \frac{3g_{\Xi\Xi}^2}{16\pi f_\pi^2} m_\pi^3 \end{aligned} \tag{26}$$

for the octet baryons and

$$\begin{aligned} m_\Delta(m_\pi) &= m_\Delta^{(0)} - 4c_\Delta^{(1)} m_\pi^2 - \frac{25}{27}\frac{g_{\Delta\Delta}^2}{16\pi f_\pi^2} m_\pi^3 \\ m_{\Sigma^*}(m_\pi) &= m_{\Sigma^*}^{(0)} - 4c_{\Sigma^*}^{(1)} m_\pi^2 - \frac{10}{9}\frac{g_{\Sigma^*\Sigma^*}^2}{16\pi f_\pi^2} m_\pi^3 \\ m_{\Xi^*}(m_\pi) &= m_{\Xi^*}^{(0)} - 4c_{\Xi^*}^{(1)} m_\pi^2 - \frac{5}{3}\frac{g_{\Xi^*\Xi^*}^2}{16\pi f_\pi^2} m_\pi^3 \\ m_\Omega(m_\pi) &= m_\Omega^{(0)} - 4c_\Omega^{(1)} m_\pi^2 \end{aligned} \tag{27}$$

for the decuplet baryons. In addition we consider the next-to-leading order SU(2) χPT results [39]. For completeness, we include the expressions in Appendix C.

We fix the nucleon axial charge g_A and pion decay constant f_π to their experimental values [we use the convention such that $f_\pi = 0.092419(7)(25)$ GeV] as was done in the case of determining the lattice spacings from fitting the nucleon mass. The remaining pion-baryon axial coupling constants are taken from the following SU(3) relations [39]:

$$\begin{aligned} &\text{Octet:} \quad g_A = D + F \qquad g_{\Sigma\Sigma} = 2F, \qquad g_{\Xi\Xi} = D - F, \qquad g_{\Lambda\Sigma} = 2D \\ &\text{Decuplet:} \quad g_{\Delta\Delta} = \mathcal{H}, \qquad g_{\Sigma^*\Sigma^*} = \frac{2}{3}\mathcal{H}, \qquad g_{\Xi^*\Xi^*} = \frac{1}{3}\mathcal{H} \\ &\text{Transition:} \quad g_{\Delta N} = \mathcal{C}, \qquad g_{\Sigma^*\Sigma} = \frac{1}{\sqrt{3}}\mathcal{C}, \qquad g_{\Xi^*\Xi} = \frac{1}{\sqrt{3}}\mathcal{C}, \qquad g_{\Lambda\Sigma^*} = -\frac{1}{\sqrt{2}}\mathcal{C}. \end{aligned} \tag{28}$$

In the octet case, once g_A is fixed, the axial coupling constants depend on a single parameter α such that $\alpha = \frac{D}{D+F}$. Its value is poorly known. It can be taken either from the quark model ($\alpha = 3/5$), from the phenomenology of semileptonic decays or from hyperon-nucleon scattering. As in Ref. [39], we take $\alpha = 0.58$ or $2D = 1.47$. The axial couplings in the decuplet case depend only on $\mathcal{H}$ for which we take the value $\mathcal{H} = 2.2$, again from Ref. [39]. This value is close to the prediction by SU(6), namely $\mathcal{H} = \frac{9}{5} g_A = 2.29$. The latter was used in a previous work [41], resulting in the same cubic term for the nucleon and Δ. When fixing the octet-decuplet transition couplings we take $\mathcal{C} = 1.48$ from Ref. [58]. Having fixed the coupling constants this way, the LO, the one-loop as well as the NLO expressions are left with $m_X^{(0)}$ and $c_X^{(1)}$ as independent fit parameters. Unlike in Ref. [39] where a universal mass parameter $m_X^{(0)}$ was used for all baryons with the same strangeness, in this work we treat all mass parameters $m_X^{(0)}$ independently. The chiral extrapolation is applied to the average over all states belonging to the same isospin multiplets, except for the charged states of the Σ, Ξ and Ξ_c where small nonzero mass differences exist due to isospin breaking effects. For these particles we first extrapolate to the continuum limit to ensure that they are degenerate and then take the average of their continuum values.

We give the fit parameters extracted from fitting our lattice results for the octet and decuplet baryons to the leading one-loop order [Eqs. (26) and (27)] and NLO [Eqs. (C1) and (C2)] in Table IX. We also show the baryon

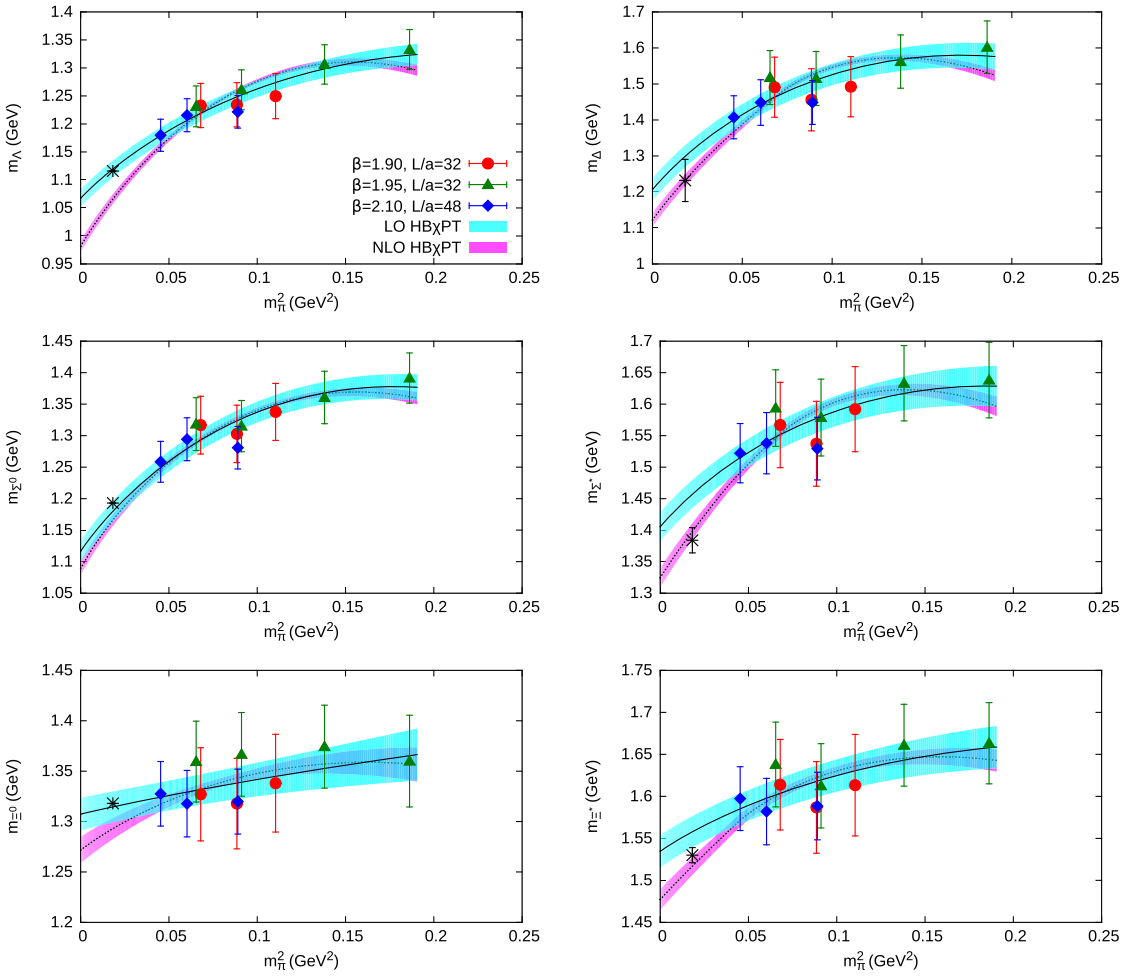

FIG. 18 (color online). Chiral extrapolations of the octet (left) and decuplet (right) baryons in physical units, using the leading one-loop expressions of Eqs. (26) and (27) respectively as well as the NLO expressions of Eqs. (C1) and (C2). The lattice values are continuum extrapolated. The notation is given in the legend in the top left plot. The experimental value is shown with the black asterisk.

masses at the physical point obtained from the leading order fits in Table XI. The lattice results for the octet and decuplet baryons at the three β values are collected in Appendix B. The deviation of the values obtained at the physical pion mass from the two fitting procedures provide an estimate of the systematic error due to the chiral extrapolation. This error on the masses is given in the second parenthesis in Table XI. Since for the Ω the LO and NLO expressions have no difference, we do not quote a systematic error due to the chiral extrapolation. We show representative plots of the chiral fits for the octet and decuplet baryons in Fig. 18. Our results shown here are continuum extrapolated and thus the errors on the points are larger than those on the raw data. The error band for the leading one-loop order and NLO fits are constructed using the super-jackknife procedure [45]. As can be seen, the data are well described by the LO fits and the physical masses of Λ, Σ^0 and Ξ^0 are reproduced. For the Δ and Ξ^* the physical point is missed by about 1 standard deviation, while the results for Σ^* extrapolate to a 5% higher value. The NLO fits also describe the lattice data satisfactory but in general extrapolate to a lower value at the physical point. Taking the difference between the value found using the LO and NLO expressions we estimate the systematic error due to the chiral extrapolation, and this yields agreement with the experimental values also in the cases of Δ, Σ^* and Ξ^*.

For the charm baryons we use the ansatz

$$m_B = m_B^{(0)} + c_1 m_\pi^2 + c_2 m_\pi^3. \tag{29}$$

This expression is motivated by SU(2) HBχPT to leading one-loop order, where $m_B^{(0)}$ and c_i are treated as independent fit parameters. As before, we add the term da^2 in the fits in order to simultaneously extrapolate to the continuum and we average over the states belonging to the same isospin multiplets. We show representative plots of the chiral fits for the charm baryons in Fig. 19. The resulting fit parameters from the fits are listed in Table X. The masses at the physical point are shown in Table XI. The lattice results

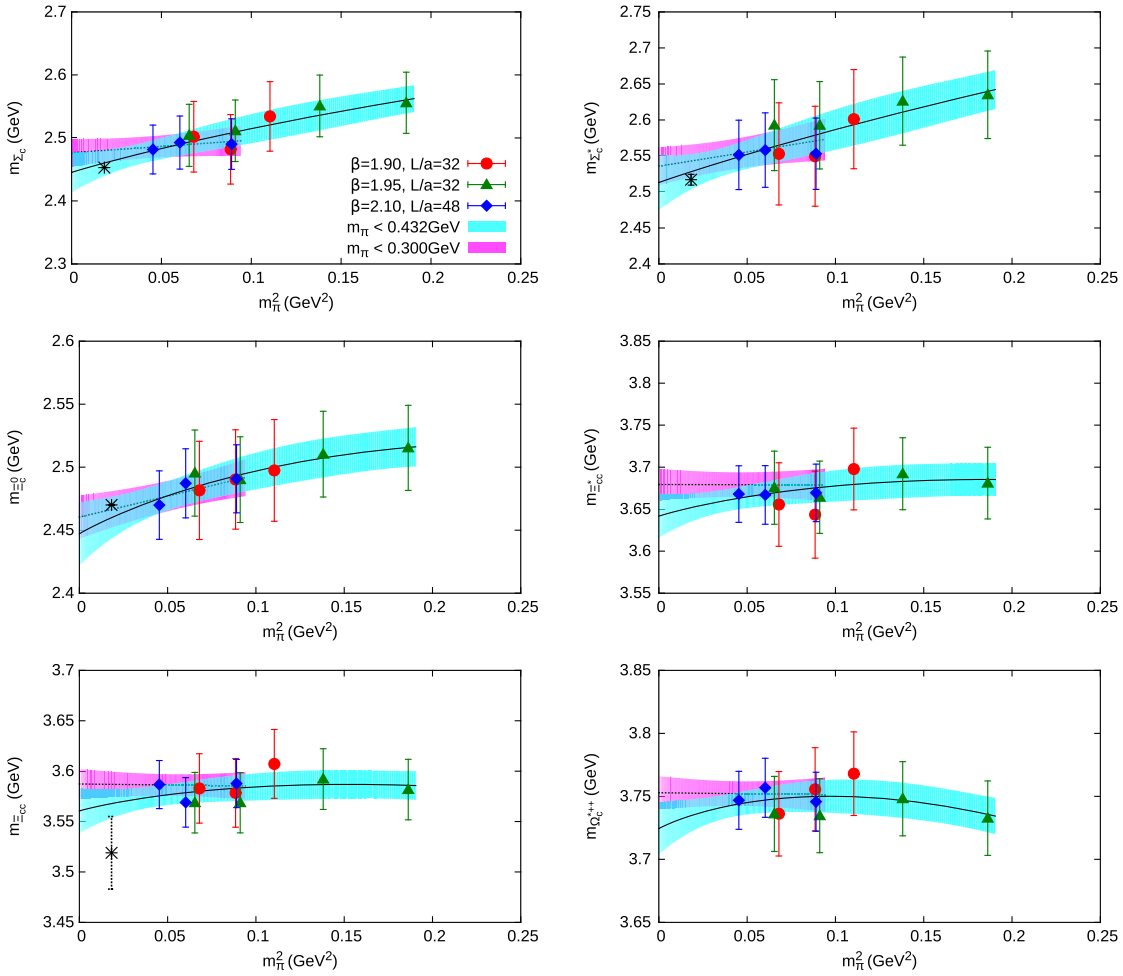

FIG. 19 (color online). Representative chiral fits of the charm spin-1/2 (left) and spin-3/2 (right) baryon results in physical units, using the ansatz of Eq. (29). The lattice results are the continuum extrapolated ones. The notation is shown in the legend of the top left plot.

for all charm baryons at the three β values are collected in Appendix B. As can be seen from the chiral fits, setting $c_2 = 0$ in the ansatz would lead to satisfactory fits as well. This is also reflected by the large uncertainties on this fit parameter, making it consistent with zero. As in the strange baryon sector, our continuum data are described well by Eq. (29), yielding values at the physical point which in general are consistent with experiment. For the Ω_c^0 and Ω_c^{*0} the lattice data extrapolate to a lower value by 1 and 2 standard deviations respectively. In order to estimate a systematic error due to the chiral extrapolation in the charm sector, we perform the chiral fits using Eq. (29) with our lattice data only up to $m_\pi \sim 300$ MeV and setting $c_2 = 0$. The deviation of the values obtained at the physical pion

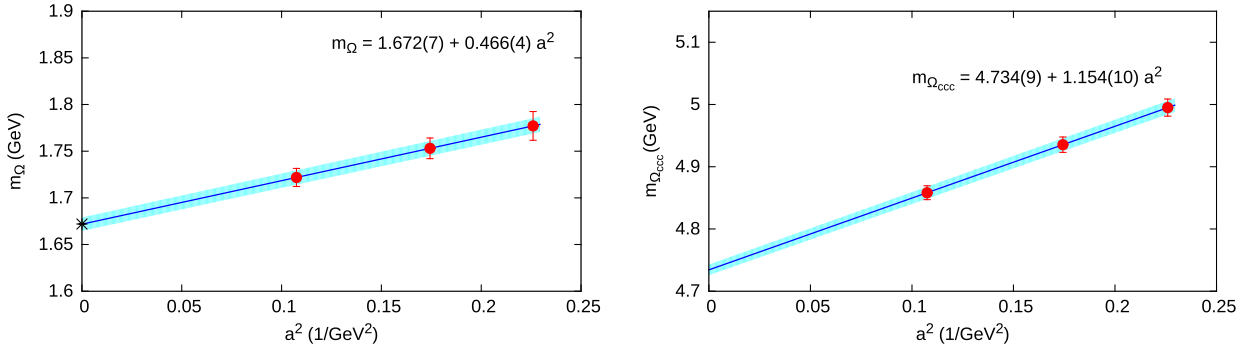

FIG. 20 (color online). Dependence of the Ω^- (left) and Ω_{ccc} (right) mass on the lattice spacing.

TABLE VIII. The value of the fit parameter d and the finite lattice spacing correction as percentage of the mass for the doubly and triply charmed baryons.

		% correction		
Baryon	d (GeV^3)	$\beta = 1.90$	$\beta = 1.95$	$\beta = 2.10$
Ξ_{cc}	1.08	6.3	5.0	3.1
Ξ^*_{cc}	1.01	5.9	4.6	2.9
Ω_{cc}	1.20	6.9	5.4	3.4
Ω^*_{cc}	1.10	6.2	4.9	3.0
Ω_{ccc}	1.15	5.1	4.1	2.6

mass from fitting using the whole pion mass range and fitting up to $m_\pi \sim 300$ MeV yields an estimation of the systematic error due to the chiral extrapolation.

The size of the cutoff effects in both the strange and charm quark sectors are small. This can be seen by the values of the fit parameter d, which are $\mathcal{O}(1)$, and thus the cutoff effects are indeed $\mathcal{O}(a^2)$. As an example, we show in Fig. 20 the a-dependence of the mass of the Ω^- and Ω_{ccc} for fixed quark masses. The correction at the largest value of a is 6% for the Ω^- and 5% for the Ω_{ccc}. In Table VIII we give the values of the parameter d and the finite lattice spacing corrections in percentage of the mass at each β value for the doubly and triply charmed-baryon masses.

We also estimate a systematic uncertainty due to the tuning for all strange and charm baryons. This is done by evaluating the baryon masses when the strange and charm quark masses take the upper and lower bound allowed by the error in their tuned values [Eq. (25)]. The deviation of the mass extracted using χPT to leading order provides an estimate of the systematic error due to the tuning, given in the third parenthesis in Table XI. In the strange sector, the systematic error due to the tuning on the strange baryon masses gives an upper bound of the error expected, since the tuning was performed using the Ω which contains three strange quarks, and thus any error due to the uncertainty of the tuning would be the largest in this case.

As in the nucleon case, an estimate of the light σ-term of all the hyperons and charmed baryons considered in this work can be made, by taking the derivative $m_\pi^2 \partial m_B / \partial m_\pi^2$. For the octet and decuplet we calculate $\sigma_{\pi B}$ using the LO as well as the NLO expressions. It is apparent that the value extracted depends on the fitting ansatz, and since the slope of the NLO fit is larger at the physical point, the resulting values for $\sigma_{\pi B}$ from the NLO expressions are larger, again indicating the sensitivity on the chiral extrapolations. We

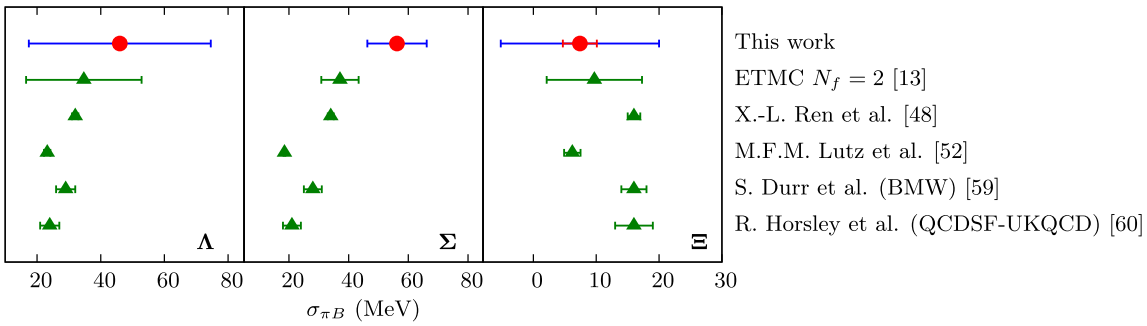

FIG. 21 (color online). Comparison of the light σ-term of the spin-1/2 hyperons in MeV, extracted from the $\mathcal{O}(p^3)$ in this work with the results from other lattice calculations. Our result shows the statistical error in red and a systematic error in blue taken as the difference between the value obtained using the $\mathcal{O}(p^3)$ and $\mathcal{O}(p^4)$ expressions [Eqs. (26) and (C1) respectively] providing an estimate of the uncertainty due to the chiral extrapolation.

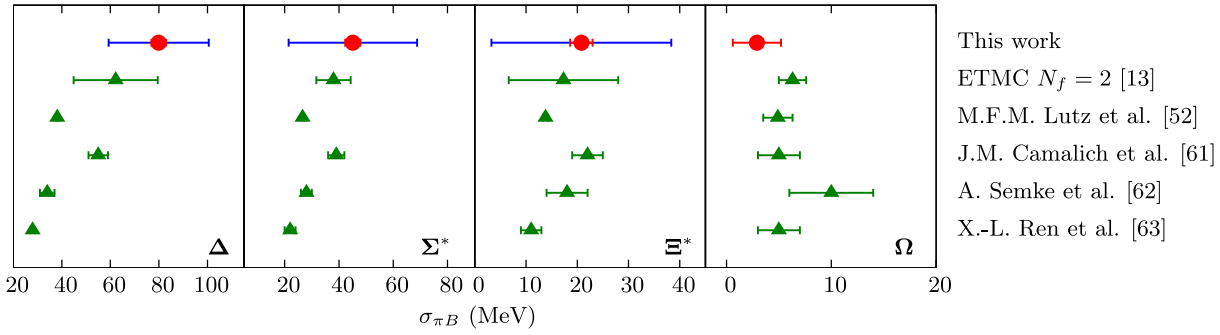

FIG. 22 (color online). Comparison of the light σ-term of the spin-3/2 hyperons in MeV, extracted from the $\mathcal{O}(p^3)$ in this work with the results from other lattice calculations. The notation is the same as that in Fig. 21.

TABLE IX. The mass at the chiral limit, $m_B^{(0)}$, and the fit parameter $c_B^{(1)}$ as determined from fitting to the leading one-loop order expressions for the octet and decuplet baryons at the tuned strange quark mass. Also shown in the value of the light σ-term at the physical point determined from the fits.

			$\sigma_{\pi B}$ (MeV)	
Baryon	$m_B^{(0)}$ (GeV)	$-4c_B^{(1)}$ (GeV^{-1})	$\mathcal{O}(p^3)$	NLO
N	0.867(2)	4.574	64.9(1.5)	45.3(4.3)
Λ	1.067(16)	3.544(97)	46.0(1.8)	74.5(1.8)
Σ^+	1.110(21)	4.470(113)	55.6(2.1)	65.3(2.2)
Σ^0	1.117(17)	4.422(95)	54.7(1.7)	64.5(1.8)
Σ^-	1.095(18)	4.618(102)	58.3(1.9)	68.3(1.9)
Ξ^0	1.307(16)	0.433(147)	6.8(2.7)	18.9(2.7)
Ξ^-	1.312(12)	0.497(107)	8.0(2.0)	20.4(1.9)
Δ	1.207(31)	6.496(162)	79.9(3.0)	100.3(3.1)
Σ^*	1.405(23)	3.603(156)	45.1(2.8)	68.6(2.7)
Ξ^*	1.535(19)	1.562(123)	20.8(2.2)	38.2(2.2)
Ω	1.669(19)	0.161(124)	2.9(2.3)	

list the values extracted for the octet and decuplet baryons in Table IX. A number of other recent works [13,48,52,59–63] have computed the light σ-terms for the octet and decuplet baryons by analyzing lattice QCD data from various collaborations. We compare our results with the results of these calculations in Figs. 21 and 22. As for the case of the nucleon σ-term, we take the difference between the values obtained using $\mathcal{O}(p^3)$ and $\mathcal{O}(p^4)$ perturbation theory as an estimate of the systematic error arising from the chiral extrapolation. This explains why our results have a larger error as compared to other groups which, typically, do not include such an estimate. Extending this analysis we can compute the poorly known σ-terms for the charmed baryons from the fitting ansatz of Eq. (29). We list the resulting values in Table X.

TABLE X. The mass at the chiral limit, $m_B^{(0)}$, and fit parameters c_i as determined from fitting to the ansatz of Eq. (29) for the charm baryons at the tuned strange and charm quark masses. Also listed is the value of the light σ-term in MeV.

Baryon	$m_B^{(0)}$ (GeV)	c_1 (GeV^{-1})	c_2 (GeV^{-2})	$\sigma_{\pi B}$ (MeV)
Λ_c	2.272(26)	0.799(935)	−0.118(1.834)	14.1(10.3)
Σ_c	2.445(32)	0.903(1.118)	−0.662(2.159)	14.0(12.4)
Ξ_c	2.469(28)	0.233(906)	−0.087(1.782)	4.6(10.0)
Ξ_c	2.447(25)	0.855(788)	−1.128(1.527)	11.4(8.8)
Ξ_c'	2.542(27)	1.242(870)	−1.924(1.690)	15.5(9.7)
Ω_c	2.629(22)	1.028(768)	−2.017(1.507)	11.3(8.5)
Ξ_{cc}	3.561(22)	0.516(725)	−0.880(1.415)	6.2(8.0)
Ω_{cc}	3.654(18)	0.341(602)	−0.937(1.193)	2.8(6.6)
Σ_c^*	2.513(38)	0.887(1.345)	−0.481(2.593)	14.4(15.0)
Ξ_c^*	2.628(33)	0.483(1.178)	−0.766(2.339)	6.0(12.9)
Ω_c^*	2.709(26)	1.408(875)	−2.623(1.710)	16.0(9.7)
Ξ_{cc}^*	3.642(26)	0.703(891)	−1.087(1.733)	8.8(9.9)
Ω_{cc}^*	3.724(21)	0.792(719)	−1.695(1.418)	8.2(7.9)
Ω_{ccc}	4.733(18)	0.156(551)	−0.443(1.082)	1.2(6.1)

TABLE XI. Our values of the masses of the baryons considered in this work after extrapolating to the physical point and taking the continuum limit given in GeV, with the associated statistical error shown in the first parenthesis. The error in the second parenthesis is an estimate of the systematic error due to the chiral extrapolation and in the third parenthesis (except for Δ, which contains only light quarks) is an estimate of the systematic error due to the tuning. There are no systematic errors for Ω^- and Λ_c^+ since these are used for the tuning of the strange and charm quark mass, respectively.

Baryon (PDG)	m (GeV)
N (0.939)	0.939
Λ (1.116)	1.120(15)(54)(22)
Σ (1.193)	1.168(32)(14)(44)
Ξ (1.318)	1.318(19)(23)(9)
Δ (1.232)	1.299(30)(66)
Σ^* (1.384)	1.457(22)(28)(32)
Ξ^* (1.530)	1.558(18)(41)(19)
Ω (1.672)	1.672(18)
Λ_c (2.286)	2.286(17)(10)
Σ_c (2.453)	2.460(20)(20)(6)
Ξ_c (2.470)	2.467(24)(4)(5)
Ξ_c' (2.575)	2.560(16)(22)(42)
Ω_c^0 (2.695)	2.643(14)(19)(42)
Ξ_{cc} (3.519)	3.568(14)(19)(1)
Ω_{cc}^+	3.658(11)(16)(50)
Σ_c^* (2.517)	2.528(25)(15)(7)
Ξ_c^* (2.645)	2.635(20)(27)(55)
Ω_c^{*0} (2.765)	2.728(16)(19)(26)
Ξ_{cc}^*	3.652(17)(27)(3)
Ω_{cc}^{*+}	3.735(13)(18)(43)
Ω_{ccc}^{++}	4.734(12)(11)(9)

It is worth mentioning that a number of analyses based on baryon chiral perturbation theory have been carried out for the octet baryon masses and sigma terms. We refer for example to Refs. [64–66] for details.

V. COMPARISON WITH RESULTS FROM OTHER COLLABORATIONS

In this section we compare our lattice results with those of other collaborations which use different discretization schemes. Having already extrapolated to the continuum, we also compare our values at the physical pion mass with the corresponding results of other collaborations and with experiment.

Several collaborations have calculated the strange spectrum. The Budapest-Marseille-Wuppertal (BMW) Collaboration carried out simulations using tree level improved 6-step stout smeared $N_f = 2 + 1$ clover fermions and a tree level Symanzik improved gauge action. The lattice spacing values used to obtain the continuum limit

were $a = 0.065$ fm, 0.085 fm and 0.125 fm. Using pion masses as low as 190 MeV, a polynomial fit was performed to extrapolate to the physical point [67]. The PACS-CS Collaboration obtained results using $N_f = 2 + 1$ nonperturbatively $\mathcal{O}(a)$ improved clover fermions on an Iwasaki gauge action on a lattice of spatial length of 2.9 fm and a value of lattice spacing $a = 0.09$ fm [68]. In addition, the octet and decuplet spectrum was obtained in Ref. [69], using $N_f = 2 + 1$ SLiNC configurations. Reference [70] also includes results on the charmed baryons from an analysis on $N_f = 2 + 1$ 2-HEX [71] and SLiNC [69,72] configurations produced by the BMW-c and QCDSF Collaborations respectively. Finally, we compare with the LHPC Collaboration, which obtained results using a hybrid action of domain wall valence quarks on a staggered sea on a lattice of spatial length 2.5 and 3.5 fm at lattice spacing $a = 0.124$ fm [73].

In Fig. 23 we compare our lattice results on the octet baryons with those of BMW, the PACS-CS and the LHPC Collaborations. In the nucleon case, we furthermore compare with results from the MILC Collaboration [74], obtained from $N_f = 2 + 1 + 1$ simulations using the one-loop Symanzik improved gauge action and an improved Kogut-Susskind quark action at a lattice spacing value $a = 0.130$ fm and with results from QCDSF-UKQCD, obtained using $N_f = 2$ simulations at three values of the lattice spacing, $a = 0.076, 0.072, 0.060$ fm [75]. We note that our results shown in these plots and the results from the PACS-CS and LHPC are not continuum extrapolated, while the results from BMW are continuum extrapolated and have larger errors than the rest. Nevertheless, there is an overall agreement, best seen in the case of the nucleon mass, which indicates that cutoff effects are small. A similar behavior is also seen in the case for the mass in the decuplet shown in Fig. 24, where we compare our results with those from PACS-CS and LHPC. We stress that these lattice results need to be extrapolated to zero lattice spacing (continuum limit) and therefore small deviations are to be expected the raw data. A comparison is also made with recent phenomenology results on the octet and decuplet baryon masses, obtained from an analysis of lattice QCD data based on the relativistic chiral Lagrangian [52]. As can be seen from Fig. 25, results show an overall agreement.

In Fig. 26 we show the masses for the octet and decuplet baryons obtained after extrapolating to the continuum limit and to the physical pion mass. Our results are obtained using the leading order expansions from HBχPT and the statistical error and total error are shown separately. The error in red in our results shown in Fig. 26 represents the statistical error. The total error bar, shown in blue, is obtained after adding quadratically the statistical error and the systematic errors due to the chiral extrapolation and due to the tuning.

In addition, we compare our results obtained in the charm sector with the corresponding results of other lattice

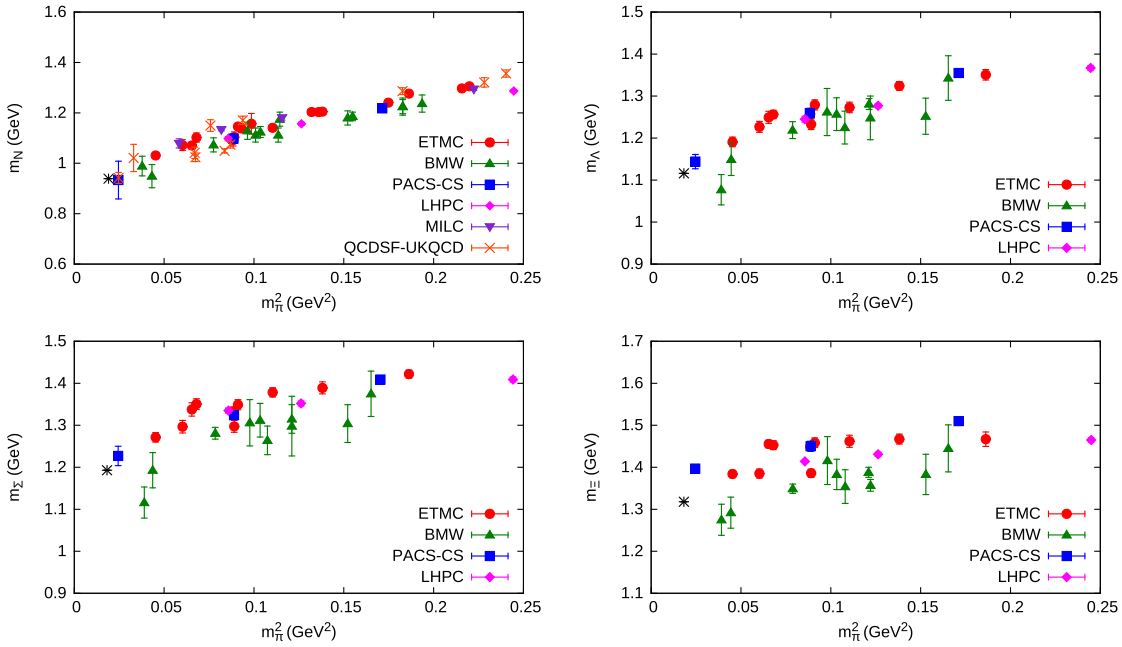

FIG. 23 (color online). Comparison of lattice results of this work (red filled circles) with those from other collaborations for the octet baryons. Results using clover fermions from BMW [67] are shown in green triangles and from PACS-CS [68] with blue squares. Domain wall valence quarks by the LHPC [73] are shown in magenta diamonds. In the nucleon case we additionally show results from the MILC Collaboration [74] in purple inverted triangles and from QCDSF-UKQCD [75] with orange crosses. The physical point is shown with the black asterisk.

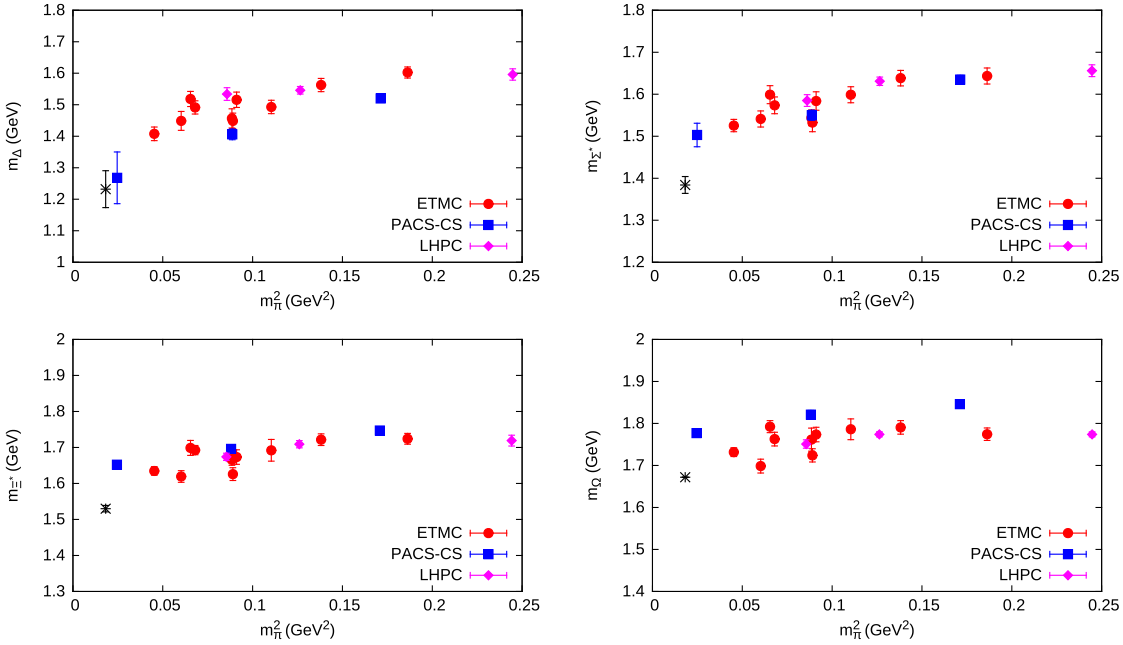

FIG. 24 (color online). Comparison of the results for the decuplet baryons in this work with the results from PACS-CS using clover fermions [68] and from the LHPC Collaboration [73] using domain wall valence quarks. The notation is as in Fig. 23.

calculations. Specifically, the MILC Collaboration has obtained results using a clover charm valence quark in $N_f = 2 + 1 + 1$ gauge configurations at three values of the lattice spacing, $a = 0.09, 0.12, 0.15$ fm [11,77]. Moreover, results for the charm spectrum were produced from $N_f = 2 + 1 + 1$ gauge configurations at lattice spacing values $a = 0.06, 0.09, 0.12$ fm using the highly improved staggered quark action, whereas the valence up, down and strange quark propagators were generated using the clover improved Wilson action [10]. A relativistic heavy quark action was implemented for the charm quark in order to reduce discretization artifacts. In Ref. [12] domain wall fermions are used for the up, down and strange quarks with $N_f = 2 + 1$ simulations using the improved Kogut-Susskind sea quarks at a lattice spacing value $a = 0.12$ fm. For the charm quark the relativistic Fermilab action was adopted. Finally, the PACS-CS has obtained results in the charm sector using the relativistic heavy quark action on $N_f = 2 + 1$ configurations with the light and strange quarks tuned to their physical masses, a lattice spacing

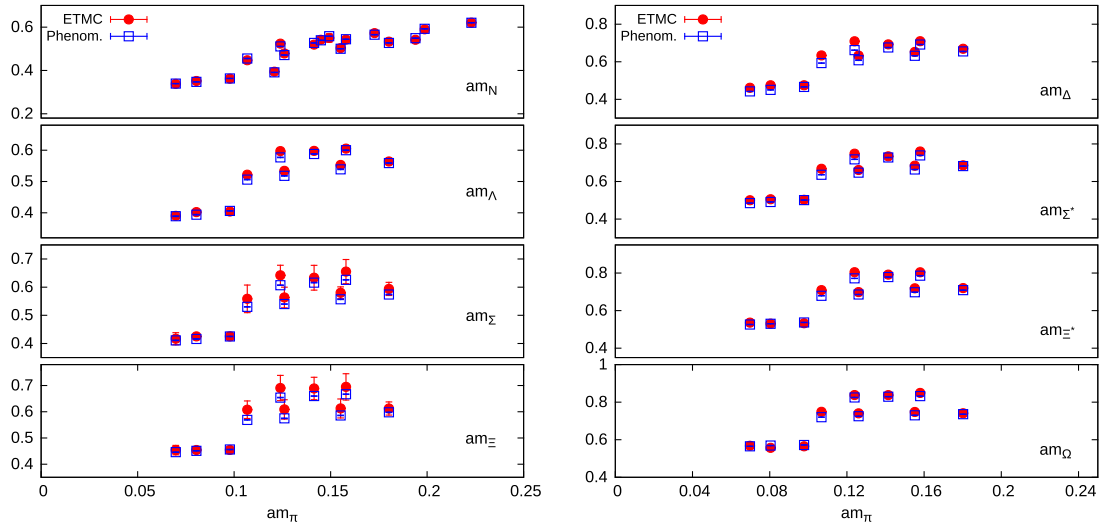

FIG. 25 (color online). Comparison of the lattice results for the octet (left) and decuplet (right) baryons from this work (red circles) with the phenomenology results from Ref. [52] (blue open squares). The results are consistent for all β values.

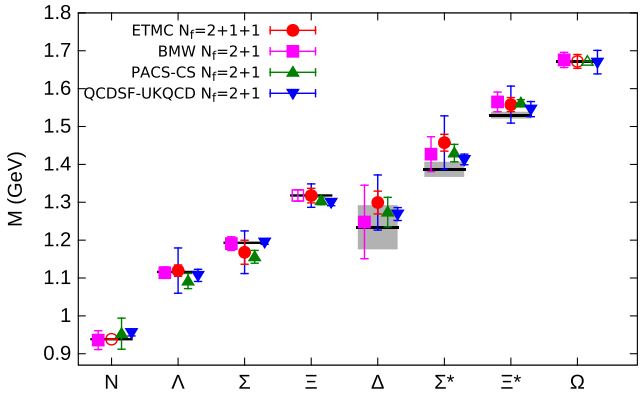

FIG. 26 (color online). The octet and decuplet baryon masses obtained at the physical point and the experimental masses [76] shown by the horizontal bands. For most baryons the band is too small to be visible. For the twisted mass results of this work (red circles) the chiral extrapolation was performed using the leading order HBχPT. In our results, the statistical error is shown in red, whereas the blue error bar includes the statistical error and the systematic errors due to the chiral extrapolation and due to the tuning added in quadrature. Results using clover fermions from BMW [67] are shown in magenta squares and from PACS-CS [68] with green triangles. Results from QCDSF-UKQCD Collaborations [69] using $N_f = 2 + 1$ SLiNC configurations are also displayed in blue inverted triangles. Open symbols are used wherever the mass was used as input to the calculations.

of $a = 0.09$ fm and a spatial length of $L = 2.9$ fm [78]. We compare our results with those from Refs. [10–12,77,78].

In Fig. 27 we compare our continuum extrapolated results on the charmed spectrum with experiment again showing separately the statistical error and the total error. Given the agreement with the experimental values, lattice QCD thus provides predictions for the mass of the Ξ_{cc}^*, Ω_{cc}, Ω_{cc}^* and Ω_{ccc}. These predictions are consistent among lattice calculations, as shown in Fig. 27. We also point out that our value for Ξ_{cc} is within errors with the value measured by the SELEX experiment.

VI. CONCLUSIONS

The twisted mass formulation allowing simulations with dynamical strange and charm quarks with their mass fixed to approximately their physical values provides a good framework for studying the baryon spectrum. A number of gauge ensembles are analyzed spanning pion masses from about 450 to 210 MeV for three lattice spacings. For the strange and charm valence quarks we use the Osterwalder-Seiler formulation and tuned their mass using the mass of the Ω and Λ_c, respectively. Thus the strange and charm quarks are treated in the same manner as the light quarks. This is to be contrasted with other lattice calculations where $N_f = 2 + 1$ staggered gauge configurations are used and the charm valence quark is introduced using a different discretization scheme such as clover or described by a relativistic heavy quark action. A comparison of our lattice results to other lattice calculations before extrapolations shows an overall similar tread for all lattice formulations.

Having values for the masses at three lattice spacings is crucial in order to both verify that cutoff effects are under control and to extrapolate the results to the continuum limit. We perform a continuum extrapolation to all our data and chiral extrapolate to the physical pion mass. In most cases, the largest systematic error arises because of the chiral extrapolation and the tuning of the strange and charm quark masses. We estimate the error due to the chiral extrapolation by comparing results at different orders of the chiral expansion. The systematic error due to tuning is estimated by varying the strange and charm quark mass within the error band of the Ω and Λ_c masses at the physical point. From the chiral fits we can determine the light σ-terms for all baryons via the Feynman-Hellmann theorem. The largest uncertainty in their determination arises from the chiral extrapolation which, in some cases amounts to over 30% error. Therefore direct determinations of the σ-terms [53,79] although very computer intensive can provide a valuable alternative. The values extracted for $\sigma_{\pi B}$ for all the baryons are given in Table IX.

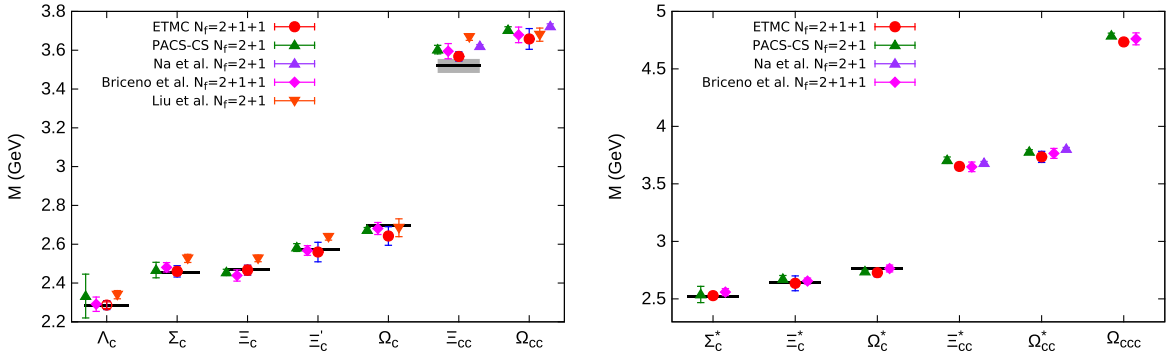

FIG. 27 (color online). The masses of spin-1/2 (left) and spin-3/2 (right) charm baryons. The notation of our results (ETMC) is the same as in Fig. 26. The experimental values are from Ref. [76] and are shown with the horizontal bands. Included are results from various hybrid actions with staggered sea quarks from Refs. [11,77] (purple triangles), [10] (magenta diamonds) and [12] (orange inverted triangles). Results from PACS-CS [78] are shown in green triangles.

Our values for the baryon masses at the physical point, shown in Figs. 26 and 27, reproduce the known baryon masses. For the Ξ_{cc} we find a mass of 3.568(14)(19)(1) GeV, which is higher by 1 standard deviation as compared with the value of 3.519 GeV measured by the SELEX Collaboration. Our prediction for the mass of the Ξ^*_{cc} is 3.652(17)(27)(3) GeV, for the Ω^+_{cc} is 3.658(11)(16)(50) GeV, for Ω^{*+}_{cc} 3.735(13)(18)(43) GeV and for Ω^{++}_{ccc} 4.734(12)(11)(9) GeV.

ACKNOWLEDGMENTS

We would like to thank all members of the ETMC for the many valuable and constructive discussions and the very fruitful collaboration that took place during the development of this work. The project used computer time granted by the John von Neumann Institute for Computing (NIC) on JUQUEEN (project hch02) and JUROPA (project ecy00) at the Jülich Supercomputing Centre as well as by the Cyprus Institute on the Cy-Tera machine (project lspro113s1), under the Cy-Tera project (NEA ΥΠΟΔΟΜΗ/ΣΤΡΑΤΗ/0308/31). We thank the staff members of these computing centers for their technical advice and support. C. K. is supported by the project GPUCW [ΤΠΕ/ΠΛΗΡΟ/0311(BIE)/09], which is co-financed by the European Regional Development Fund and the Republic of Cyprus through the Research Promotion Foundation.

APPENDIX A: INTERPOLATING FIELDS FOR BARYONS

In Tables XII, XIII, and XIV, we give the interpolating fields for the baryons used in this work in correspondence with Fig. 2 and Fig. 3. Throughout, C denotes the charge conjugation matrix and spinor indices are suppressed.

TABLE XII. Interpolating fields and quantum numbers for the $20'$-plet of spin-1/2 baryons.

Charm	Strange	Baryon	Quark content	Interpolating field	I	I_z
$c=2$	$s=0$	Ξ^{++}_{cc}	ucc	$\epsilon_{abc}(c_a^T C\gamma_5 u_b)c_c$	1/2	+1/2
		Ξ^{+}_{cc}	dcc	$\epsilon_{abc}(c_a^T C\gamma_5 d_b)c_c$	1/2	−1/2
	$s=1$	Ω^{+}_{cc}	scc	$\epsilon_{abc}(c_a^T C\gamma_5 s_b)c_c$	0	0
$c=1$		Λ^+_c	udc	$\frac{1}{\sqrt{6}}\epsilon_{abc}[2(u_a^T C\gamma_5 d_b)c_c + (u_a^T C\gamma_5 c_b)d_c - (d_a^T C\gamma_5 c_b)u_c]$	0	0
	$s=0$	Σ^{++}_c	uuc	$\epsilon_{abc}(u_a^T C\gamma_5 c_b)u_c$	1	+1
		Σ^{+}_c	udc	$\frac{1}{\sqrt{2}}\epsilon_{abc}[(u_a^T C\gamma_5 c_b)d_c + (d_a^T C\gamma_5 c_b)u_c]$	1	0
		Σ^{0}_c	ddc	$\epsilon_{abc}(d_a^T C\gamma_5 c_b)d_c$	1	−1
	$s=1$	Ξ^{+}_c	usc	$\epsilon_{abc}(u_a^T C\gamma_5 s_b)c_c$	1/2	+1/2
		Ξ^{0}_c	dsc	$\epsilon_{abc}(d_a^T C\gamma_5 s_b)c_c$	1/2	−1/2
		Ξ'^{+}_c	usc	$\frac{1}{\sqrt{2}}\epsilon_{abc}[(u_a^T C\gamma_5 c_b)s_c + (s_a^T C\gamma_5 c_b)u_c]$	1/2	+1/2
		Ξ'^{0}_c	dsc	$\frac{1}{\sqrt{2}}\epsilon_{abc}[(d_a^T C\gamma_5 c_b)s_c + (s_a^T C\gamma_5 c_b)d_c]$	1/2	−1/2
	$s=2$	Ω^{0}_c	ssc	$\epsilon_{abc}(s_a^T C\gamma_5 c_b)s_c$	0	0
$c=0$	$s=0$	p	uud	$\epsilon_{abc}(u_a^T C\gamma_5 d_b)u_c$	1/2	+1/2
		n	udd	$\epsilon_{abc}(d_a^T C\gamma_5 u_b)d_c$	1/2	−1/2
		Λ	uds	$\frac{1}{\sqrt{6}}\epsilon_{abc}[2(u_a^T C\gamma_5 d_b)s_c + (u_a^T C\gamma_5 s_b)d_c - (d_a^T C\gamma_5 s_b)u_c]$	0	0
	$s=1$	Σ^{+}	uus	$\epsilon_{abc}(u_a^T C\gamma_5 s_b)u_c$	1	+1
		Σ^{0}	uds	$\frac{1}{\sqrt{2}}\epsilon_{abc}[(u_a^T C\gamma_5 s_b)d_c + (d_a^T C\gamma_5 s_b)u_c]$	1	0
		Σ^{-}	dds	$\epsilon_{abc}(d_a^T C\gamma_5 s_b)d_c$	1	−1
	$s=2$	Ξ^{0}	uss	$\epsilon_{abc}(s_a^T C\gamma_5 u_b)s_c$	1/2	+1/2
		Ξ^{-}	dss	$\epsilon_{abc}(s_a^T C\gamma_5 d_b)s_c$	1/2	−1/2

TABLE XIII. Interpolating fields and quantum numbers for the 20-plet of spin-3/2 baryons.

Charm	Strange	Baryon	Quark content	Interpolating field	I	I_z
$c=3$	$s=0$	Ω_{ccc}^{++}	ccc	$\epsilon_{abc}(c_a^T C\gamma_\mu c_b)c_c$	0	0
$c=2$	$s=0$	$\Xi_{cc}^{\star++}$	ucc	$\epsilon_{abc}(c_a^T C\gamma_\mu u_b)c_c$	1/2	+1/2
		$\Xi_{cc}^{\star+}$	dcc	$\epsilon_{abc}(c_a^T C\gamma_\mu d_b)c_c$	1/2	−1/2
	$s=1$	$\Omega_{cc}^{\star+}$	scc	$\epsilon_{abc}(c_a^T C\gamma_\mu s_b)c_c$	0	0
$c=1$	$s=0$	$\Sigma_c^{\star++}$	uuc	$\frac{1}{\sqrt{3}}\epsilon_{abc}[(u_a^T C\gamma_\mu u_b)c_c + 2(c_a^T C\gamma_\mu u_b)u_c]$	1	+1
		$\Sigma_c^{\star+}$	udc	$\sqrt{\frac{2}{3}}\epsilon_{abc}[(u_a^T C\gamma_\mu d_b)c_c + (d_a^T C\gamma_\mu c_b)u_c + (c_a^T C\gamma_\mu u_b)d_c]$	1	0
		$\Sigma_c^{\star0}$	ddc	$\frac{1}{\sqrt{3}}\epsilon_{abc}[(d_a^T C\gamma_\mu d_b)c_c + 2(c_a^T C\gamma_\mu d_b)d_c]$	1	−1
	$s=1$	$\Xi_c^{\star+}$	usc	$\epsilon_{abc}(s_a^T C\gamma_\mu u_b)c_c$	1/2	+1/2
		$\Xi_c^{\star0}$	dsc	$\epsilon_{abc}(s_a^T C\gamma_\mu d_b)c_c$	1/2	−1/2
	$s=2$	$\Omega_c^{\star0}$	ssc	$\epsilon_{abc}(s_a^T C\gamma_\mu c_b)s_c$	0	0
$c=0$	$s=0$	Δ^{++}	uuu	$\epsilon_{abc}(u_a^T C\gamma_\mu u_b)u_c$	3/2	+3/2
		Δ^{+}	uud	$\frac{1}{\sqrt{3}}\epsilon_{abc}[2(u_a^T C\gamma_\mu d_b)u_c + (u_a^T C\gamma_\mu u_b)d_c]$	3/2	+1/2
		Δ^{0}	udd	$\frac{1}{\sqrt{3}}\epsilon_{abc}[2(d_a^T C\gamma_\mu u_b)d_c + (d_a^T C\gamma_\mu d_b)u_c]$	3/2	−1/2
		Δ^{-}	ddd	$\epsilon_{abc}(d_a^T C\gamma_\mu d_b)d_c$	3/2	−3/2
	$s=1$	$\Sigma^{\star+}$	uus	$\frac{1}{\sqrt{3}}\epsilon_{abc}[(u_a^T C\gamma_\mu u_b)s_c + 2(s_a^T C\gamma_\mu u_b)u_c]$	1	+1
		$\Sigma^{\star0}$	uds	$\sqrt{\frac{2}{3}}\epsilon_{abc}[(u_a^T C\gamma_\mu d_b)s_c + (d_a^T C\gamma_\mu s_b)u_c + (s_a^T C\gamma_\mu u_b)d_c]$	1	0
		$\Sigma^{\star-}$	dds	$\frac{1}{\sqrt{3}}\epsilon_{abc}[(d_a^T C\gamma_\mu d_b)s_c + 2(s_a^T C\gamma_\mu d_b)d_c]$	1	−1
	$s=2$	$\Xi^{\star0}$	uss	$\epsilon_{abc}(s_a^T C\gamma_\mu u_b)s_c$	1/2	+1/2
		$\Xi^{\star-}$	dss	$\epsilon_{abc}(s_a^T C\gamma_\mu d_b)s_c$	1/2	−1/2
	$s=3$	Ω^{-}	sss	$\epsilon_{abc}(s_a^T C\gamma_\mu s_b)s_c$	0	0

TABLE XIV. Additional interpolating fields for spin-1/2 and spin-3/2 baryons. There are two of the spin-1/2 baryons and eight of the spin-3/2 baryons.

Charm	Strange	Baryon	Quark content	Interpolating field	I	I_z
				Spin-1/2 baryons		
$c=1$	$s=1$	Ξ_c^{+}	usc	$\frac{1}{\sqrt{6}}\epsilon_{abc}[2(s_a^T C\gamma_5 u_b)c_c + (s_a^T C\gamma_5 c_b)u_c - (u_a^T C\gamma_5 c_b)s_c]$	1/2	+1/2
		Ξ_c^{0}	dsc	$\frac{1}{\sqrt{6}}\epsilon_{abc}[2(s_a^T C\gamma_5 d_b)c_c + (s_a^T C\gamma_5 c_b)d_c - (d_a^T C\gamma_5 c_b)s_c]$	1/2	−1/2
				Spin-3/2 baryons		
$c=0$	$s=2$	$\Xi^{\star0}$	uss	$\frac{1}{\sqrt{3}}\epsilon_{abc}[2(s_a^T C\gamma_\mu u_b)s_c + (s_a^T C\gamma_\mu s_b)u_c]$	1/2	+1/2
		$\Xi^{\star-}$	dss	$\frac{1}{\sqrt{3}}\epsilon_{abc}[2(s_a^T C\gamma_\mu d_b)s_c + (s_a^T C\gamma_\mu s_b)d_c]$	1/2	−1/2
$c=1$	$s=1$	$\Xi_c^{\star+}$	usc	$\sqrt{\frac{2}{3}}\epsilon_{abc}[(u_a^T C\gamma_\mu s_b)c_c + (s_a^T C\gamma_\mu c_b)u_c + (c_a^T C\gamma_\mu u_b)s_c]$	1/2	+1/2
		$\Xi_c^{\star0}$	dsc	$\sqrt{\frac{2}{3}}\epsilon_{abc}[(d_a^T C\gamma_\mu s_b)c_c + (s_a^T C\gamma_\mu c_b)d_c + (c_a^T C\gamma_\mu d_b)s_c]$	1/2	−1/2
	$s=2$	$\Omega_c^{\star0}$	ssc	$\frac{1}{\sqrt{3}}\epsilon_{abc}[2(s_a^T C\gamma_\mu c_b)s_c + (s_a^T C\gamma_\mu s_b)c_c]$	0	0
$c=2$	$s=0$	$\Xi_{cc}^{\star++}$	ucc	$\frac{1}{\sqrt{3}}\epsilon_{abc}[2(c_a^T C\gamma_\mu u_b)c_c + (c_a^T C\gamma_\mu c_b)u_c]$	1/2	+1/2
		$\Xi_{cc}^{\star+}$	dcc	$\frac{1}{\sqrt{3}}\epsilon_{abc}[2(c_a^T C\gamma_\mu d_b)c_c + (c_a^T C\gamma_\mu c_b)d_c]$	1/2	−1/2
	$s=1$	$\Omega_{cc}^{\star+}$	scc	$\frac{1}{\sqrt{3}}\epsilon_{abc}[2(c_a^T C\gamma_\mu s_b)c_c + (c_a^T C\gamma_\mu c_b)s_c]$	0	0

APPENDIX B: LATTICE RESULTS

In Tables XV, XVI, XVII, XVIII, XIX, and XX we list the baryon masses in lattice units and the continuum extrapolated values in physical units. The masses in physical units are in GeV and are converted from lattice units using the lattice spacing values extracted from the nucleon in this work, Eq. (21). The masses for the nucleon Ω and Λ_c^+ are listed in Tables III and VI.

TABLE XV. Octet and decuplet baryon masses in lattice units with the associated statistical error.

$a\mu_l$	am_Λ	am_Σ	am_Ξ	am_Δ	am_{Σ^*}	am_{Ξ^*}
			$\beta = 1.90$			
0.0030	0.5972(46)	0.6420(60)	0.6906(50)	0.7090(100)	0.7481(95)	0.8046(61)
0.0040	0.5978(46)	0.6335(52)	0.6888(38)	0.6924(145)	0.7339(89)	0.7918(73)
0.0050	0.6051(60)	0.6552(52)	0.6949(69)	0.7097(101)	0.7600(91)	0.8044(144)
			$\beta = 1.95$			
0.0025	0.5217(59)	0.5586(66)	0.6077(38)	0.6340(100)	0.6677(89)	0.7093(87)
0.0035	0.5341(50)	0.5633(50)	0.6090(48)	0.6329(102)	0.6614(92)	0.6987(84)
0.0055	0.5529(43)	0.5800(60)	0.6126(50)	0.6525(88)	0.6841(77)	0.7189(68)
0.0075	0.5640(52)	0.5937(39)	0.6125(72)	0.6691(74)	0.6862(80)	0.7199(62)
			$\beta = 2.10$			
0.0015	0.3904(37)	0.4167(37)	0.4537(28)	0.4614(71)	0.5000(48)	0.5359(39)
0.0020	0.4021(43)	0.4250(49)	0.4540(35)	0.4749(98)	0.5052(63)	0.5308(53)
0.0030	0.4041(40)	0.4253(46)	0.4543(32)	0.4749(81)	0.5024(71)	0.5330(58)

TABLE XVI. Octet and decuplet baryon masses in physical units with the associated statistical error.

$a\mu_l$	m_Λ	m_Σ	m_Ξ	m_Δ	m_{Σ^*}	m_{Ξ^*}
			$\beta = 1.90$			
0.0030	1.2329(394)	1.3103(435)	1.3331(356)	1.4909(834)	1.5669(678)	1.6139(539)
0.0040	1.2343(394)	1.2924(431)	1.3294(349)	1.4560(863)	1.5372(674)	1.5869(545)
0.0050	1.2496(402)	1.3381(431)	1.3422(369)	1.4923(835)	1.5920(675)	1.6133(604)
			$\beta = 1.95$			
0.0025	1.2314(364)	1.3067(399)	1.3632(312)	1.5178(749)	1.5938(608)	1.6379(504)
0.0035	1.2610(356)	1.3180(385)	1.3662(320)	1.5152(750)	1.5787(610)	1.6126(502)
0.0055	1.3063(351)	1.3580(393)	1.3748(322)	1.5621(740)	1.6332(598)	1.6609(487)
0.0075	1.3328(358)	1.3909(378)	1.3746(345)	1.6019(731)	1.6382(600)	1.6633(483)
			$\beta = 2.10$			
0.0015	1.1798(287)	1.2522(308)	1.3272(250)	1.4074(598)	1.5222(470)	1.5973(380)
0.0020	1.2157(294)	1.2775(324)	1.3282(258)	1.4484(632)	1.5380(486)	1.5819(395)
0.0030	1.2216(291)	1.2783(320)	1.3290(253)	1.4484(609)	1.5294(497)	1.5885(402)

TABLE XVII. Charm spin-1/2 baryon masses in lattice units with the associated statistical error.

$a\mu_l$	am_{Σ_c}	am_{Ξ_c}	$am_{\Xi_c'}$	$am_{\Omega_c^0}$	$am_{\Xi_{cc}}$	$am_{\Omega_{cc}^+}$
			$\beta = 1.90$			
0.0030	1.2543(72)	1.2611(46)	1.3028(53)	1.3575(46)	1.8187(48)	1.8704(38)
0.0040	1.2448(53)	1.2580(62)	1.2983(50)	1.3506(37)	1.8166(42)	1.8694(33)
0.0050	1.2696(55)	1.2599(61)	1.3185(49)	1.3655(47)	1.8303(44)	1.8781(37)
			$\beta = 1.95$			
0.0025	1.0896(55)	1.0900(43)	1.1388(42)	1.1764(41)	1.5684(34)	1.6099(29)
0.0035	1.0927(49)	1.0920(41)	1.1322(43)	1.1726(39)	1.5684(32)	1.6077(27)
0.0055	1.1091(51)	1.1027(37)	1.1440(44)	1.1788(39)	1.5782(36)	1.6138(33)
0.0075	1.1112(43)	1.1024(36)	1.1412(37)	1.1691(37)	1.5739(34)	1.6065(34)
			$\beta = 2.10$			
0.0015	0.8348(35)	0.8362(25)	0.8682(27)	0.9010(23)	1.2136(25)	1.2449(19)
0.0020	0.8384(64)	0.8419(33)	0.8735(35)	0.9000(30)	1.2078(31)	1.2414(21)
0.0030	0.8376(49)	0.8410(26)	0.8741(33)	0.9028(28)	1.2139(25)	1.2438(19)

TABLE XVIII. Charm spin-1/2 baryon masses in physical units with the associated statistical error.

$a\mu_l$	m_{Σ_c}	m_{Ξ_c}	$m_{\Xi_c'}$	$m_{\Omega_c^0}$	$m_{\Xi_{cc}}$	$m_{\Omega_{cc}^+}$
			$\beta = 1.90$			
0.0030	2.5020(560)	2.4921(374)	2.5890(412)	2.6663(350)	3.5829(344)	3.6631(268)
0.0040	2.4820(551)	2.4856(384)	2.5796(410)	2.6518(345)	3.5784(340)	3.6611(265)
0.0050	2.5342(552)	2.4896(384)	2.6221(410)	2.6831(350)	3.6072(341)	3.6794(267)
			$\beta = 1.95$			
0.0025	2.5042(492)	2.4865(334)	2.6102(363)	2.6713(311)	3.5687(300)	3.6461(235)
0.0035	2.5114(489)	2.4912(332)	2.5946(364)	2.6623(310)	3.5687(299)	3.6408(234)
0.0055	2.5509(490)	2.5168(330)	2.6228(364)	2.6771(310)	3.5921(301)	3.6554(238)
0.0075	2.5558(485)	2.5161(329)	2.6160(360)	2.6538(309)	3.5818(300)	3.6378(239)
			$\beta = 2.10$			
0.0015	2.4816(387)	2.4746(261)	2.5766(286)	2.6585(242)	3.5867(239)	3.6686(186)
0.0020	2.4927(421)	2.4921(269)	2.5927(294)	2.6557(249)	3.5690(245)	3.6581(188)
0.0030	2.4902(401)	2.4891(262)	2.5944(292)	2.6643(247)	3.5877(239)	3.6652(186)

TABLE XIX. Charm spin-3/2 baryon masses in lattice units with the associated statistical error.

$a\mu_l$	$am_{\Sigma_c^*}$	$am_{\Xi_c^*}$	$am_{\Omega_c^{*0}}$	$am_{\Xi_{cc}^*}$	$am_{\Omega_{cc}^{*+}}$	$am_{\Omega_{ccc}^{++}}$
			$\beta = 1.90$			
0.0030	1.2828(103)	1.3333(78)	1.3780(58)	1.8464(71)	1.8941(47)	2.3788(37)
0.0040	1.2812(76)	1.3337(57)	1.3846(48)	1.8407(100)	1.9034(38)	2.3845(48)
0.0050	1.3057(65)	1.3543(57)	1.3953(51)	1.8665(52)	1.9092(41)	2.3857(42)
			$\beta = 1.95$			
0.0025	1.1296(90)	1.1757(52)	1.2049(46)	1.6084(54)	1.6400(41)	2.0486(29)
0.0035	1.1295(53)	1.1588(63)	1.1999(46)	1.6037(45)	1.6394(35)	2.0537(27)
0.0055	1.1435(63)	1.1767(54)	1.2028(51)	1.6153(42)	1.6451(36)	2.0578(29)
0.0075	1.1471(54)	1.1608(64)	1.2016(43)	1.6107(39)	1.6386(38)	2.0570(28)
			$\beta = 2.10$			
0.0015	0.8591(41)	0.8951(32)	0.9239(28)	1.2380(26)	1.2669(21)	1.5958(20)
0.0020	0.8612(73)	0.8928(53)	0.9277(30)	1.2377(40)	1.2702(26)	1.5928(20)
0.0030	0.8596(55)	0.8909(44)	0.9296(29)	1.2384(33)	1.2665(26)	1.5946(16)

TABLE XX. Charm spin-3/2 baryon masses in physical units with the associated statistical error.

$a\mu_l$	$m_{\Sigma_c^*}$	$m_{\Xi_c^*}$	$m_{\Omega_c^{*0}}$	$m_{\Xi_{cc}^*}$	$m_{\Omega_{cc}^{*+}}$	$m_{\Omega_{ccc}^{++}}$
			$\beta = 1.90$			
0.0030	2.5529(709)	2.6263(552)	2.7461(402)	3.6555(497)	3.7362(335)	4.7432(263)
0.0040	2.5496(694)	2.6271(541)	2.7599(396)	3.6435(518)	3.7556(330)	4.7552(270)
0.0050	2.6012(689)	2.6704(541)	2.7824(397)	3.6978(486)	3.7680(332)	4.7576(266)
			$\beta = 1.95$			
0.0025	2.5928(631)	2.6778(479)	2.7677(354)	3.6756(436)	3.7361(298)	4.7049(231)
0.0035	2.5927(607)	2.6373(487)	2.7557(353)	3.6642(430)	3.7347(293)	4.7171(229)
0.0055	2.6261(612)	2.6803(481)	2.7626(357)	3.6921(428)	3.7481(294)	4.7268(231)
0.0075	2.6349(607)	2.6422(488)	2.7600(351)	3.6810(427)	3.7327(295)	4.7250(230)
			$\beta = 2.10$			
0.0015	2.5515(482)	2.6459(377)	2.7459(277)	3.6679(336)	3.7469(230)	4.7443(183)
0.0020	2.5581(517)	2.6388(398)	2.7576(279)	3.6669(349)	3.7568(234)	4.7350(184)
0.0030	2.5530(495)	2.6329(387)	2.7632(278)	3.6694(342)	3.7457(234)	4.7406(180)

APPENDIX C: HBχPT NEXT-TO-LEADING ORDER EXPRESSIONS FOR THE OCTET AND DECUPLET BARYONS

For the octet baryons the NLO expressions read

$$\begin{aligned}
m_\Lambda^{\mathrm{NLO}}(m_\pi) &= m_\Lambda^{(0)} - 4c_\Lambda^{(1)} m_\pi^2 - \frac{g_{\Lambda\Sigma}^2}{(4\pi f_\pi)^2}\mathcal{F}(m_\pi, \Delta_{\Lambda\Sigma}, \lambda) \\
&\quad - \frac{4g_{\Lambda\Sigma^*}^2}{(4\pi f_\pi)^2}\mathcal{F}(m_\pi, \Delta_{\Lambda\Sigma^*}, \lambda) \\
m_\Sigma^{\mathrm{NLO}}(m_\pi) &= m_\Sigma^{(0)} - 4c_\Sigma^{(1)} m_\pi^2 - \frac{2g_{\Sigma\Sigma}^2}{16\pi f_\pi^2} m_\pi^3 \\
&\quad - \frac{g_{\Lambda\Sigma}^2}{3(4\pi f_\pi)^2}\mathcal{F}(m_\pi, -\Delta_{\Lambda\Sigma}, \lambda) \\
&\quad - \frac{4g_{\Sigma^*\Sigma}^2}{3(4\pi f_\pi)^2}\mathcal{F}(m_\pi, \Delta_{\Sigma\Sigma^*}, \lambda) \\
m_\Xi^{\mathrm{NLO}}(m_\pi) &= m_\Xi^{(0)} - 4c_\Xi^{(1)} m_\pi^2 - \frac{3g_{\Xi\Xi}^2}{16\pi f_\pi^2} m_\pi^3 \\
&\quad - \frac{2g_{\Xi^*\Xi}^2}{(4\pi f_\pi)^2}\mathcal{F}(m_\pi, \Delta_{\Xi\Xi^*}, \lambda)
\end{aligned} \tag{C1}$$

and for the decuplet baryons

$$\begin{aligned}
m_\Delta^{\mathrm{NLO}}(m_\pi) &= m_\Delta^{(0)} - 4c_\Delta^{(1)} m_\pi^2 - \frac{25}{27}\frac{g_{\Delta\Delta}^2}{16\pi f_\pi^2} m_\pi^3 \\
&\quad - \frac{2g_{\Delta N}^2}{3(4\pi f_\pi)^2}\mathcal{F}(m_\pi, -\Delta_{N\Delta}, \lambda) \\
m_{\Sigma^*}^{\mathrm{NLO}}(m_\pi) &= m_{\Sigma^*}^{(0)} - 4c_{\Sigma^*}^{(1)} m_\pi^2 - \frac{10}{9}\frac{g_{\Sigma^*\Sigma^*}^2}{16\pi f_\pi^2} m_\pi^3 \\
&\quad - \frac{2}{3(4\pi f_\pi)^2}[g_{\Sigma^*\Sigma}^2\mathcal{F}(m_\pi, -\Delta_{\Sigma\Sigma^*}, \lambda) \\
&\quad + g_{\Lambda\Sigma^*}^2\mathcal{F}(m_\pi, -\Delta_{\Lambda\Sigma^*}, \lambda)] \\
m_{\Xi^*}^{\mathrm{NLO}}(m_\pi) &= m_{\Xi^*}^{(0)} - 4c_{\Xi^*}^{(1)} m_\pi^2 - \frac{5}{3}\frac{g_{\Xi^*\Xi^*}^2}{16\pi f_\pi^2} m_\pi^3 \\
&\quad - \frac{g_{\Xi^*\Xi}^2}{(4\pi f_\pi)^2}\mathcal{F}(m_\pi, -\Delta_{\Xi\Xi^*}, \lambda) \\
m_\Omega^{\mathrm{NLO}}(m_\pi) &= m_\Omega^{(0)} - 4c_\Omega^{(1)} m_\pi^2.
\end{aligned} \tag{C2}$$

The nonanalytic function $\mathcal{F}(m, \Delta, \lambda)$ is of the form [58]

$$\begin{aligned}
\mathcal{F}(m, \Delta, \lambda) &= (m^2 - \Delta^2)\sqrt{\Delta^2 - m^2 + i\epsilon} \\
&\quad \times \log\left(\frac{\Delta - \sqrt{\Delta^2 - m^2 + i\epsilon}}{\Delta + \sqrt{\Delta^2 - m^2 + i\epsilon}}\right) \\
&\quad - \frac{3}{2}\Delta m^2 \log\left(\frac{m^2}{\lambda^2}\right) - \Delta^3 \log\left(\frac{4\Delta^2}{m^2}\right)
\end{aligned} \tag{C3}$$

depending on the threshold parameter $\Delta_{XY} = m_Y^{(0)} - m_X^{(0)}$ and on the scale λ of chiral perturbation theory, fixed to $\lambda = 1$ GeV. For $\Delta > 0$ the real part of the function $\mathcal{F}(m, \Delta, \lambda)$ has the property

$$\mathcal{F}(m, -\Delta, \lambda) = \begin{cases} -\mathcal{F}(m, \Delta, \lambda) & m < \Delta \\ -\mathcal{F}(m, \Delta, \lambda) + 2\pi(m^2 - \Delta^2)^{3/2} & m > \Delta \end{cases} \tag{C4}$$

which corrects a typo in the sign of the second term in Ref. [73].

A noticeable result of this expansion is the absence of a cubic term in the expressions for the Λ and Ω baryons given in Eqs. (C1) and (C2). In the case of Ω it follows from the absence of light valence quarks. However, the absence of a cubic term in the NLO expression for Λ, although a consequence of χPT, is nevertheless a questionable result, since it relies on the assumption that $m_\pi \ll M_\Sigma - M_\Lambda$. In the limit $\Delta \to 0$ the nonanalytic function of Eq. (C3) becomes

$$\mathcal{F}(m_\pi, \Delta \to 0, \lambda) = \pi m_\pi^3, \tag{C5}$$

which generates a cubic term for the Λ and slightly modifies the existing one for Σ. The corresponding expressions are given by

$$\begin{aligned}
m_\Lambda(m_\pi) &= m_\Lambda^{(0)} - 4c_\Lambda^{(1)} m_\pi^2 - \frac{g_{\Lambda\Sigma}^2}{16\pi f_\pi^2} m_\pi^3 \\
m_\Sigma(m_\pi) &= m_\Sigma^{(0)} - 4c_\Sigma^{(1)} m_\pi^2 - \frac{2g_{\Sigma\Sigma}^2 + g_{\Lambda\Sigma}^2/3}{16\pi f_\pi^2} m_\pi^3.
\end{aligned} \tag{C6}$$

[1] M. Mattson *et al.* (SELEX Collaboration), Phys. Rev. Lett. **89**, 112001 (2002).
[2] J. Russ (SELEX Collaboration), arXiv:hep-ex/0209075.
[3] A. Ocherashvili *et al.* (SELEX Collaboration), Phys. Lett. B **628**, 18 (2005).
[4] B. Aubert *et al.* (*BABAR* Collaboration), Phys. Rev. D **74**, 011103 (2006).
[5] R. Chistov *et al.* (BELLE Collaboration), Phys. Rev. Lett. **97**, 162001 (2006).
[6] W. Roberts and M. Pervin, Int. J. Mod. Phys. **A23**, 2817 (2008).
[7] A. Martynenko, Phys. Lett. B **663**, 317 (2008).
[8] D. Ebert, R. Faustov, V. Galkin, and A. Martynenko, Phys. Rev. D **66**, 014008 (2002).

[9] Z.-G. Wang, Eur. Phys. J. A **45**, 267 (2010).
[10] R. A. Briceno, H.-W. Lin, and D. R. Bolton, Phys. Rev. D **86**, 094504 (2012).
[11] H. Na and S. Gottlieb, *Proc. Sci.*, LATTICE2008 (2008) 119.
[12] L. Liu, H.-W. Lin, K. Orginos, and A. Walker-Loud, Phys. Rev. D **81**, 094505 (2010).
[13] C. Alexandrou, R. Baron, J. Carbonell, V. Drach, P. Guichon, K. Jansen, T. Korzec, and O. Pène (ETM Collaboration), Phys. Rev. D **80**, 114503 (2009).
[14] R. Frezzotti and G. Rossi, *Proc. Sci.*, LAT2007 (2007) 277.
[15] P. Dimopoulos *et al.* (ETM Collaboration), *Proc. Sci.*, LATTICE2008 (2008) 103.
[16] K. Jansen, *Proc. Sci.*, LATTICE2008 (2008) 010.
[17] C. Alexandrou, EPJ Web Conf. **73**, 01013 (2014).
[18] R. Frezzotti, P. A. Grassi, S. Sint, and P. Weisz (Alpha Collaboration), J. High Energy Phys. 08 (2001) 058.
[19] P. Weisz, Nucl. Phys. **B212**, 1 (1983).
[20] R. Frezzotti and G. Rossi, J. High Energy Phys. 08 (2004) 007.
[21] R. Frezzotti and G. Rossi, J. High Energy Phys. 10 (2004) 070.
[22] R. Frezzotti and G. Rossi, Nucl. Phys. B, Proc. Suppl. **128**, 193 (2004).
[23] P. Boucaud *et al.* (ETM Collaboration), Comput. Phys. Commun. **179**, 695 (2008).
[24] R. Frezzotti, G. Martinelli, M. Papinutto, and G. Rossi, J. High Energy Phys. 04 (2006) 038.
[25] R. Baron, P. Boucaud, J. Carbonell, A. Deuzeman, V. Drach *et al.*, J. High Energy Phys. 06 (2010) 111.
[26] A. Athenodorou and R. Sommer, Phys. Lett. B **705**, 393 (2011).
[27] B. Blossier *et al.* (ETM Collaboration), J. High Energy Phys. 04 (2008) 020.
[28] B. Blossier *et al.* (European Twisted Mass Collaboration), J. High Energy Phys. 07 (2009) 043.
[29] A. M. Abdel-Rehim, R. Lewis, R. Woloshyn, and J. M. Wu, Eur. Phys. J. A **31**, 773 (2007).
[30] A. M. Abdel-Rehim, R. Lewis, R. Woloshyn, and J. M. Wu, Phys. Rev. D **74**, 014507 (2006).
[31] B. Ioffe, Nucl. Phys. **B188**, 317 (1981).
[32] D. B. Leinweber, R. Woloshyn, and T. Draper, Phys. Rev. D **43**, 1659 (1991).
[33] D. B. Leinweber, T. Draper, and R. Woloshyn, Phys. Rev. D **46**, 3067 (1992).
[34] S. Durr, G. Koutsou, and T. Lippert, Phys. Rev. D **86**, 114514 (2012).
[35] S. Gusken, Nucl. Phys. B, Proc. Suppl. **17**, 361 (1990).
[36] C. Alexandrou, S. Gusken, F. Jegerlehner, K. Schilling, and R. Sommer, Nucl. Phys. **B414**, 815 (1994).
[37] M. Benmerrouche, R. Davidson, and N. Mukhopadhyay, Phys. Rev. C **39**, 2339 (1989).
[38] J. Zanotti, D. Leinweber, A. Williams, J. Zhang, W. Melnitchouk, and S. Choe (CSSM Lattice Collaboration), Phys. Rev. D **68**, 054506 (2003).
[39] B. C. Tiburzi and A. Walker-Loud, Phys. Lett. B **669**, 246 (2008).
[40] J. Gasser, M. Sainio, and A. Svarc, Nucl. Phys. **B307**, 779 (1988).
[41] C. Alexandrou *et al.* (European Twisted Mass Collaboration), Phys. Rev. D **78**, 014509 (2008).
[42] V. Bernard, T. R. Hemmert, and U.-G. Meissner, Phys. Lett. B **622**, 141 (2005).
[43] V. Pascalutsa and M. Vanderhaeghen, Phys. Lett. B **636**, 31 (2006).
[44] M. Procura, B. Musch, T. Wollenweber, T. Hemmert, and W. Weise, Phys. Rev. D **73**, 114510 (2006).
[45] J. Bratt *et al.* (LHPC Collaboration), Phys. Rev. D **82**, 094502 (2010).
[46] R. Baron *et al.* (ETM Collaboration), *Proc. Sci.*, LATTICE2010 (2010) 123.
[47] J. Alarcon, J. Martin Camalich, and J. Oller, Phys. Rev. D **85**, 051503 (2012).
[48] X.-L. Ren, L.-S. Geng, and J. Meng, arXiv:1404.4799.
[49] J. Gasser, H. Leutwyler, and M. Sainio, Phys. Lett. **B253**, 252 (1991).
[50] G. S. Bali *et al.* (QCDSF Collaboration), Phys. Rev. D **85**, 054502 (2012).
[51] L. Alvarez-Ruso, T. Ledwig, J. Martin Camalich, and M. Vicente-Vacas, Phys. Rev. D **88**, 054507 (2013).
[52] M. Lutz, R. Bavontaweepanya, C. Kobdaj, and K. Schwarz, Phys. Rev. D **90**, 054505 (2014).
[53] A. Abdel-Rehim, C. Alexandrou, M. Constantinou, V. Drach, K. Hadjiyiannakou, K. Jansen, G. Koutsou, and A. Vaquero, Phys. Rev. D **89**, 034501 (2014).
[54] N. Carrasco, A. Deuzeman, P. Dimopoulos, R. Frezzotti, V. Gimenez *et al.*, Nucl. Phys. **B887**, 19 (2014).
[55] C. Alexandrou, J. Carbonell, D. Christaras, V. Drach, M. Gravina, and M. Papinutto, Phys. Rev. D **86**, 114501 (2012).
[56] M. Nagels, T. Rijken, J. De Swart, G. Oades, J. Petersen *et al.*, Nucl. Phys. **B147**, 189 (1979).
[57] M. Nagels, T. Rijken, and J. de Swart, Phys. Rev. D **20**, 1633 (1979).
[58] B. C. Tiburzi and A. Walker-Loud, Nucl. Phys. **A764**, 274 (2006).
[59] S. Durr, Z. Fodor, T. Hemmert, C. Hoelbling, J. Frison *et al.*, Phys. Rev. D **85**, 014509 (2012).
[60] R. Horsley, Y. Nakamura, H. Perlt, D. Pleiter, P. E. L. Rakow, G. Schierholz, A. Schiller, H. Stüben, F. Winter, and J. M. Zanotti (QCDSF-UKQCD Collaborations), Phys. Rev. D **85**, 034506 (2012).
[61] J. Martin Camalich, L. Geng, and M. Vicente Vacas, Phys. Rev. D **82**, 074504 (2010).
[62] A. Semke and M. Lutz, Phys. Lett. B **717**, 242 (2012).
[63] X.-L. Ren, L.-S. Geng, and J. Meng, Phys. Rev. D **89**, 054034 (2014).
[64] M. Frink and U.-G. Meissner, J. High Energy Phys. 07 (2004) 028.
[65] M. Frink, U.-G. Meissner, and I. Scheller, Eur. Phys. J. A **24**, 395 (2005).
[66] V. Bernard, D. Hoja, U.-G. Meissner, and A. Rusetsky, J. High Energy Phys. 06 (2009) 061.
[67] S. Durr, Z. Fodor, J. Frison, C. Hoelbling, R. Hoffmann *et al.*, Science **322**, 1224 (2008).
[68] S. Aoki *et al.* (PACS-CS Collaboration), Phys. Rev. D **79**, 034503 (2009).
[69] W. Bietenholz, V. Bornyakov, M. Gockeler, R. Horsley, W. Lockhart *et al.*, Phys. Rev. D **84**, 054509 (2011).
[70] G. Bali, S. Collins, and P. Perez-Rubio, J. Phys. Conf. Ser. **426**, 012017 (2013).

[71] S. Dürr, Z. Fodor, C. Hoelbling, S. D. Katz, S. Krieg, T. Kurth, L. Lellouch, T. Lippert, K. K. Szabó, and G. Vulvert, J. High Energy Phys. 08 (2011) 148.
[72] W. Bietenholz, V. Bornyakov, N. Cundy, M. Gockeler, R. Horsley *et al.*, Phys. Lett. B **690**, 436 (2010).
[73] A. Walker-Loud, H.-W. Lin, D. Richards, R. Edwards, M. Engelhardt *et al.*, Phys. Rev. D **79**, 054502 (2009).
[74] C. Bernard, T. Burch, K. Orginos, D. Toussaint, T. DeGrand, C. DeTar, S. Datta, S. Gottlieb, U. Heller, and R. Sugar, Phys. Rev. D **64**, 054506 (2001).
[75] G. Bali, P. Bruns, S. Collins, M. Deka, B. Glasle *et al.*, Nucl. Phys. **B866**, 1 (2013).
[76] K. Hagiwara *et al.* (Particle Data Group), Phys. Rev. D **66**, 010001 (2002).
[77] H. Na and S. A. Gottlieb, *Proc. Sci.*, LAT2007 (2007) 124.
[78] Y. Namekawa *et al.* (PACS-CS Collaboration), Phys. Rev. D **87**, 094512 (2013).
[79] C. Alexandrou, K. Hadjiyiannakou, K. Jansen, and C. Kallidonis, *Proc. Sci.*, LATTICE2013 (2013) 279.